

European Journal of Phycology

ISSN: 0967-0262 (Print) 1469-4433 (Online) Journal homepage: www.tandfonline.com/journals/tejp20

Taxonomic implications of revealing dimorphism in the Pyrenomonadaceae (Cryptophyceae): how many genera?

Maria Saburova, Antonina N. Khanaychenko, Olga V. Nikolaeva, Olga A. Rylkova, Tatiana Efimova, Mariia Berdieva, Yakov Meger & Vladimir V. Aleoshin

To cite this article: Maria Saburova, Antonina N. Khanaychenko, Olga V. Nikolaeva, Olga A. Rylkova, Tatiana Efimova, Mariia Berdieva, Yakov Meger & Vladimir V. Aleoshin (20 Aug 2026): Taxonomic implications of revealing dimorphism in the Pyrenomonadaceae (Cryptophyceae): how many genera?, European Journal of Phycology, DOI: 10.1080/09670262.2026.2696474

To link to this article: https://doi.org/10.1080/09670262.2026.2696474

View supplementary material

Published online: 20 Aug 2026.

Submit your article to this journal

View related articles

View Crossmark data

Full Terms & Conditions of access and use can be found at
https://www.tandfonline.com/action/journalInformation?journalCode=tejp20

EUROPEAN JOURNAL OF PHYCOLOGY, 2026
https://doi.org/10.1080/09670262.2026.2696474

Check for updates

Taxonomic implications of revealing dimorphism in the Pyrenomonadaceae (Cryptophyceae): how many genera?

Maria Saburova [a], Antonina N. Khanaychenko [b], Olga V. Nikolaeva[c], Olga A. Rylkova [b], Tatiana Efimova [b], Mariia Berdieva [d], Yakov Meger [b] and Vladimir V. Aleoshin [c,e,f]

[a]Coastal and Marine Resources Program, Environment and Life Sciences Research Center, Kuwait Institute for Scientific Research, P.O. BOX 1638, Salmiya 22017, Kuwait; [b]A.O. Kovalevsky Institute of Biology of the Southern Seas, Russian Academy of Sciences, Leninskii Ave., 38/3, Moscow 119991, Russian Federation; [c]Belozersky Institute for Physico-Chemical Biology, Lomonosov Moscow State University, Leninskye Gory, 1/40, Moscow 119991, Russian Federation; [d]Institute of Cytology of the Russian Academy of Sciences, St. Petersburg 194064, Russian Federation; [e]Faculty of Biology, Lomonosov Moscow State University, Leninskye Gory, 1/12, Moscow 119991, Russian Federation; [f]Kharkevich Institute for Information Transmission Problems, Russian Academy of Sciences, Bolshoy Karetny per., 19/1, Moscow 127051, Russian Federation

ABSTRACT

The present study reevaluates the taxonomy of the Pyrenomonadaceae through an integrative approach, combining molecular phylogeny with detailed morphological analysis. By expanding taxon sampling and focusing on morphologically validated strains, this research addresses long-standing conflicts between traditional phenotypic markers and emerging genetic data. The congruence of key morphological traits delineating genera with molecular phylogenies inferred from the nuclear 18S rDNA, ITS/5.8S rDNA, 28S rDNA and nucleomorph 18S rDNA was assessed. Molecular evidence confirmed dimorphism within the Pyrenomonadaceae, revealing genetically identical pairs with distinct vestibular invagination and the inner periplast morphology. In addition, comprehensive examination of three novel cryptophyte strains isolated from the Black Sea, employing LM, SEM, flow cytometry and molecular phylogeny revealed that the transition between sheet-like and plate-like inner periplast components is strictly correlated with cell ploidy levels rather than evolutionary divergence. These findings confirm a dimorphic (haploid-diploid) life cycle within the family. The genetic identity between morphologically disparate morphotypes justifies the abolition of the genus *Storeatula*, relegating it to a life-cycle stage of other related genera. A revision of the Pyrenomonadaceae was performed to fill the gap in its classification according to the latest morphological and molecular phylogenetic findings, resulting in the erection of a novel genus, *Eomonas* gen. nov. accommodating previously recognized and two newly described taxa from the Black Sea, *Eomonas fusiformis* sp. nov. and *Eomonas vitalis* sp. nov. Furthermore, we address the nomenclatural challenges posed by the poorly defined type species, *Rhodomonas baltica*, which currently prevents a complete formal revision of the family. To navigate this instability, we introduce a set of unique molecular signatures that allow for robust species delineation regardless of morphological or life-cycle stage state. This study emphasizes a transition in cryptophyte systematics towards a diagnostic framework that prioritizes stable genomic and ploidy-related characters over plastic phenotypic traits.

HIGHLIGHTS

- Taxonomic reliability of traits within Pyrenomonadaceae was evaluated.
- Dimorphism was inferred by phylogenetic and cytological tools across Pyrenomonadaceae.
- *Eomonas* gen. nov., here erected, accommodates taxa distantly related to *Rhodomonas*.

ARTICLE HISTORY Received 3 September 2025; Revised 8 June 2026; Accepted 19 June 2026

KEYWORDS Black Sea; compensatory base changes; cryptophyte; dimorphism; ITS2; Pyrenomonadaceae; rDNA phylogeny; revision; taxonomy

Introduction

Cryptophycean flagellates have been studied since the 19th century, when Christian Gottfried Ehrenberg prophetically named them 'cryptomonads' in 1831 (Ehrenberg, 1832, cited after Daugbjerg & Devantier, 2024). Nearly 200 years later, their classification and taxonomy remain unresolved, mainly as a result of the variability in morphological and biochemical characteristics, as well as the heteromorphy found in the life cycle of some species (Hill & Wetherbee, 1986; Hoef-Emden & Melkonian, 2003; Hoef-Emden & Archibald, 2017; Altenburger *et al.*, 2020; Hoef-Emden *et al.*, 2024). Research on cryptophytes in the Black Sea began in 1918 with the discovery of several taxa in a saltwater lake in Crimea, including *Cryptomonas stigmatica* (Wisłouch, 1924), later redescribed as *Rhodomonas stigmatica* in Australia (Hill, 1991). Other Black Sea species, such as *C. rubra* and *C. vulgaris* (Rouchijajnen, 1967, 1970), were assigned to *Cryptomonas* based on light microscopy (LM). However, their original descriptions lack consistency, and the absence of holotype material prevents formal taxonomic reevaluation. Nevertheless, recent checklists (Moncheva *et al.*, 2001; Lazăr *et al.*, 2018;

CONTACT Maria Saburova msaburova@gmail.com
© 2026 British Phycological Society

Published online 20 Aug 2026

Mikaelyan *et al.*, 2021) continue to erroneously assign Black Sea marine cryptophytes to this strictly freshwater genus (Hoef-Emden & Melkonian, 2003; Hoef-Emden, 2007; Gusev *et al.*, 2022).

The initial classic approach to identify cryptophytes relied on morphological features observed under LM, which offered limited resolution and insufficient differentiation between species. This approach was based on the shape and dimensions of live cells, the presence and number of plastids, the location of the pyrenoid and nucleus, and the presence of either a tubular gullet lined with large explosive ejectosomes, or a gullet-furrow combination (Butcher, 1967; Hill & Wetherbee, 1989; Kugrens *et al.*, 1999). Later, with the advent of electron microscopy, the taxonomic keys and systematics of cryptophytes were supplemented with ultrastructural features unique to cryptophytes, and studied by scanning electron microscopy (SEM) externally and by transmission electron microscopy (TEM) internally. These include the nature of the internal periplast component, the location and shape of the pyrenoid and nucleomorph, the appearance of the gullet-furrow complex and the rhizostyle (e.g. Gillott & Gibbs, 1980; Clay *et al.*, 1999; Majaneva *et al.*, 2014). Despite the variation in cell colour with growth conditions and culture age, the genetic expression of a specific accessory pigment (phycobiliprotein) type remains a consistent biochemical trait (Klaveness, 1985) and serves as a stable, albeit genus-overlapping, taxonomic marker (Klaveness, 1985; Hill & Rowan, 1989; Cunningham *et al.*, 2019; Greenwold *et al.*, 2023).

A molecular approach to study cryptophytes has proven instrumental in elucidating their unique biology, revealing hidden diversity and evolutionary history beyond traditional morphology-based taxonomy. However, the advent of molecular genetics gave rise to new complications, including conflicts between traditional systematics based on morphological characters, and molecular phylogenetic analysis. Recent molecular studies (ITS and SSU/LSU rDNA) have revealed that traditional phenotypic markers for cryptophyte delineation, such as cell size and shape, periplast plates, and pyrenoid presence/number, are either highly variable or life-history dependent. Since these morphological traits conflict with genetic data, several genera and species have been reduced to synonyms. Consequently, a reevaluation of cryptophyte classification ensued, with the incorporation of genetic markers as key diagnostic characters (Deane *et al.*, 2002; Hoef-Emden *et al.*, 2002; Hoef-Emden & Melkonian, 2003; Hoef-Emden, 2007, 2018; Lane & Archibald, 2008; Majaneva *et al.*, 2014; Hoef-Emden & Archibald, 2017; Gusev *et al.*, 2020, 2022; Khanaychenko *et al.*, 2022; Martynenko *et al.*, 2022; Daugbjerg & Devantier, 2024).

The discovery of a dimorphic (haploid-diploid) life cycle alternating between sheet-like and plated periplast stages has triggered taxonomic revisions in cryptophytes. This dimorphism has initially been observed in *Proteomonas sulcata* Hill & Wetherbee 1986, in which a single clonal culture displayed a larger diploid form with a continuous sheet-like inner periplast and a smaller haploid form with discrete hexagonal periplast plates and half of the DNA content (Hill & Wetherbee, 1986). Subsequent integrated molecular and morphological studies have revealed similar dimorphism in other cryptophytes previously misidentified as distinct genera or species. Consequently, the genera *Campylomonas* Hill 1991 and *Chilomonas* Ehrenberg 1832 were synonymized with *Cryptomonas* (Hoef-Emden & Melkonian, 2003), two distinct morphotypes were linked in *Geminigera cryophila* (D.L.Taylor & C.C.Lee) Hill 1991 (van den Hoff *et al.*, 2020), and *Plagioselmis prolonga* Butcher *ex* G.Novarino, I.A.N.Lucas & S.Morrall 1994 was recognized as the haploid stage of, and synonymized with, *Teleaulax amphioxeia* (W.Conrad) Hill 1992 (Altenburger *et al.*, 2020).

The establishment of a consistent system for cryptophytes is further constrained by the intricate taxonomic history of this group. Throughout decades of research, the classification of cryptophytes has undergone several in-depth revisions (e.g. Pascher, 1914; Pringsheim, 1944; Christensen, 1962; Butcher, 1967; Bourrelly, 1970; Santore, 1984; Cavalier-Smith, 1993; Novarino & Lucas, 1993; Clay *et al.*, 1999), resulting in a substantial accumulation of synonyms in taxonomic literature and culture collection catalogues. Furthermore, many cryptophycean taxa are described based on strains for which molecular data are lacking. Conversely, nucleotide sequences deposited in public databases such as GenBank often lack detailed morphological observations for the corresponding strains, thereby preventing the reliable assignment of species names.

The Pyrenomonadaceae G.Novarino & I.A.N. Lucas 1993 notably exemplifies the complexity of cryptophyte classification, particularly in the context of the transition from morphology-based taxonomy to molecular analysis, highlighting issues such as the unresolved synonymy of certain taxa (e.g. *Rhodomonas*/*Pyrenomonas* debated), morphological plasticity and hidden dimorphism. The diagnostic character of the family is defined by a unique combination of the nucleomorph position within a pyrenoid invagination and the presence of phycobiliprotein PE-545 (Novarino & Lucas, 1993; Clay *et al.*, 1999; Deane *et al.*, 2002; Solarska *et al.*, 2023). Currently, the family comprises four genera, distinguished through conventional classification that prioritizes cell shape, the structure of vestibular invagination (gullet-furrow complex) and periplast

ultrastructure, namely *Rhodomonas* Karsten 1898/ *Pyrenomonas* Santore 1984, *Rhinomonas* D.R.A.Hill & R.Wetherbee 1988 and *Storeatula* D.R.A.Hill 1991. However, sequences assigned to *Rhodomonas*, *Pyrenomonas, Rhinomonas* and *Storeatula* form paraphyletic groups lacking consistent pattern in phylogenetic trees (Deane *et al*., 2002; Hoef-Emden *et al*., 2002; Lane *et al*., 2005; Shalchian-Tabrizi *et al*., 2008; Cunningham *et al*., 2019; Daugbjerg & Devantier, 2024). Beyond potential misidentifications, the revealed paraphyly may suggest that *Storeatula* represents an alternate life-cycle morph of other genera rather than a distinct taxonomic entity (Hoef-Emden *et al*., 2002; Hoef-Emden & Melkonian, 2003; Majaneva *et al*., 2014). Such systematic instability necessitates a transition from phenotypic taxonomy to an integrative approach to resolve long-standing diagnostic confusion.

The present study evaluated the taxonomic reliability of morphological traits currently used to differentiate genera and species within the Pyrenomonadaceae. We conducted an extensive survey of taxonomic literature, culture collections' catalogues and genetic databases to link morphology-based and molecular datasets by tracking species synonymy and strain origins. To improve phylogenetic resolution, we expanded the taxon sampling with an emphasis on morphologically validated strains. In order to discern hidden dimorphism in the Pyrenomonadaceae, the consistency of key morphological characters delineating genera within the family was assessed in congruence with molecular phylogenies inferred from the nuclear (SSU, ITS and LSU), and nucleomorph (SSU) rDNA sequences. In addition, the morphology and phylogeny of three novel cryptophyte strains isolated from the Black Sea were described based on light and electron microscopy observation of their cell morphology, pigment analysis, and nuclear and nucleomorph rDNA gene sequences. For two of these strains exhibiting a *Storeatula*-like morphology, dimorphism was suspected and cell ploidy was tested to clarify their life-history stages. Based on this integrative approach, a taxonomic revision of the family was performed, including the establishment of a novel genus.

Materials and methods

Strains origin and isolation

The characterization of hidden Black Sea cryptomonad biodiversity is an ongoing effort involving clonal cultures isolated from the coastal waters and maintained in the recently established collection of the A. O. Kovalevsky Institute of Biology of the Southern Seas (IBSS) (Khanaychenko *et al*., 2022, 2024). Novel cryptomonad strains IBSS-Cr-4.19, IBSS-Cr-4.2G and IBSS-Cr-7S4 were isolated from the shallow coastal waters over sandy sediments in the NW Black Sea, Kazachya Bay, Crimean Peninsula in October 2020 by Antonina Khanaychenko, Vitaly Giragosov and Dmitry Moiseenko (IBSS). The unpreserved samples were transferred to the laboratory, concentrated by mild reverse filtration, and examined under an inverted microscope (Nikon Eclipse MS100, Tokyo, Japan). Single-cell isolation by micropipetting was applied to establish the cryptophyte cultures. Since isolation, the strains were subsequently sub-cultured several times to purify them.

Culture maintenance

Non-axenic clonal cultures of the strains IBSS-Cr -4.19, IBSS-Cr-4.2G and IBSS-Cr-7S4 were deposited in Culture Collection of Marine Cryptophytes (CCMC) at the IBSS, where they were routinely maintained under natural photoperiod at a reduced natural light intensity of ~5–10 μE m^{-2} s^{-1} and at a temperature of 22 ± 2°C. The stock cultures were sub-cultured by diluting them by 20–50% with Walne medium prepared with sterilized seawater (salinity of 18) once per month to support exponential growth (Andersen, 2005), until the morphological and molecular analyses of the strains were conducted.

Light microscopy

The cells were observed and measured while alive to prevent the shrinkage that may occur after fixation (Novarino, 2005). Observations were conducted under inverted microscopes Nikon Eclipse MS 100 and Nikon Eclipse TS2R (Nikon Metrology NV) and upright microscope Olympus CX41 (Olympus Corporation, Japan) equipped with a Nomarski differential interference contrast (DIC) optic. Images were taken with an Olympus CX41-Infinity digital camera at a magnification of 600×.

Electron microscopy

For scanning electron microscopy (SEM), 2 ml of the dense strains IBSS-Cr-4.19, IBSS-Cr-4.2G and IBSS-Cr -7S4 cultures were fixed for 60 min in a 1% Lugol's solution (Bistricki & Munawar, 1978; Dolgin & Adolf, 2019). After fixation, the sample was gently concentrated under a vacuum of <0.2 atm onto a polycarbonate filter (2 μm pore size, Dubna, Russia) in a filter funnel (Sartorius, Germany). After precipitation on the filter, the cells were rinsed three times with distilled water and then gradually dehydrated through an ethanol series (30% and 50% for 5 min, 75% and 96% for 10 min, and 100% twice for 10 min). The filters were dried using an automated critical point dryer Leica EM CPD300 (Leica Microsystems, Germany) for 1.5–2.5 h. The dried

filters were mounted on aluminium stubs with carbon adhesive tabs and sputter-coated with Au/Pd using vacuum coater Leica EM ACE200 for 1 min before visualization with a Hitachi SU3500 (Hitachi High Tech, Japan) scanning electron microscope.

For transmission electron microscopy (TEM), algal cell suspensions of the dense strains IBSS-Cr-4.19 and IBSS-Cr-4.2G were collected by centrifugation at 2000 × g for 6 min, followed by an additional centrifugation at 3000 × g for 4 min after adding extra culture volume. The obtained pellet was fixed in 2.5% glutaraldehyde at 4°C for 1 h. All fixatives were prepared in 0.1 M cacodylate buffer containing 0.25 M sucrose, which was also used for rinsing. After three rinses, cells were post-fixed in 2% osmium tetroxide at 4°C for 1 h. Samples were then rinsed in cacodylate buffer with decreasing sucrose concentrations (0.25 M, 0.15 M and 0.05 M). The pellet was embedded in 2% agar and dehydrated through a graded ethanol series, followed by a propylene oxide-ethanol mixture and pure propylene oxide. Specimens were subsequently infiltrated with propylene oxide-resin mixtures and embedded in an Epon 812-Araldite M resin mixture (Fluka, Switzerland). Ultrathin sections were cut using an Ultracut E ultramicrotome (Reichert Jung, Austria), contrasted with uranyl acetate and lead citrate, and examined using a Libra 120 transmission electron microscope (Carl Zeiss, Germany).

Spectrophotometry

Light absorption spectra of the cells ($a_{ph}(\lambda)$) were measured in accordance with protocol (IOCCG Protocol Series, 2018). Algal cultures of 10 ml were filtered under a low vacuum (<25 kPa) through Whatman GF/F filters with a pore size 0.7 µm. Absorbance was measured over the spectral region 400–750 nm with a LAMBDA 35 (PerkinElmer) dual-beam UV/Vis spectrometer equipped with an integrating sphere. The accuracy of measurements was ± 0.5% (PerkinElmer, Inc, 2000).

Flow cytometry

The assessment of cell ploidy in three cryptophyte strains, IBSS-Cr-7S4, IBSS-Cr-4.2G and IBSS-Cr-4.19, was performed using flow cytometry. To distinguish between haploid and diploid stages, DNA content was quantified by measuring the fluorescence intensity of cells stained with a nucleic acid dye. Subsamples (15 ml) were isolated from dense cultures in the exponential growth phase, centrifuged (3000 × g, 5 min), and the resulting pellets were transferred to Eppendorf tubes. The resuspended material was stained with SYBR Green I (Invitrogen, USA) at a 1× final concentration for 30 min in the dark. Samples were analysed using a LongCyte C2050 flow cytometer (Challenbio, China) using a blue laser (488 nm) for excitation and a fluorescein isothiocyanate detection channel (FITC) (530/30 nm filter) for emission. Data were acquired at a flow rate of 50 µl min^{-1} with a 250 mV detector gain. The ploidy level was determined using the SYBR Green I fluorescence intensity in the FITC-A channel as a proxy for the amount of DNA in the cells.

DNA extraction, PCR and sequencing

DNAs were extracted from the strains IBSS-Cr-4.19, IBSS-Cr-4.2G and IBSS-Cr-7S4 using a DIAtom DNA Prep Kit (Isogen, Russia), following the manufacturer's protocol. Partial nuclear-encoded 18S (SSU) and 28S (LSU) rDNA, complete 5.8S rDNA and internal transcribed spacers (ITS1 and ITS2) regions, and partial 18S nucleomorph rDNA were amplified using novel and previously described primers (Table 1) with an Encyclo PCR Kit (Evrogen, Russia). The PCR cycling conditions included an initial denaturation step at 95°C for 5 min, followed by 40 cycles of denaturation at 95°C for 30 s, annealing at 55°C for 30 s, extension at 72°C for 3 min, and final extension at 72°C for 5 min. The PCR products were separated with agarose gel electrophoresis and purified with a Cleanup Mini Kit (Evrogen, Russia). Amplicons were sequenced directly with an Applied Biosystems 3730 DNA Analyser. The sequences were deposited in GenBank under accession numbers PP578204–PP578206 for nuclear rDNA and PV939379–PV939381 for nucleomorph rDNA.

Phylogenetic analyses

To clarify the phylogenetic placement of the strains IBSS-Cr-4.19, IBSS-Cr-4.2G and IBSS-Cr-7S4, we

Table 1. Primers used for PCR and sequencing.

Gene	Primer	Sequence	Reference
18S	A	5′-GTATCTGGTTGATCCTGCCAGT-3′	Medlin *et al.* (1988)
18S	d6	5′-CCGTTCTTAGTTGGTGG-3′	Simdyanov *et al.* (2015)
18S	d71	5′-GTCCCTGCCCTTTGTACACACCGCCCG-3′	Simdyanov *et al.* (2017)
28S	NLR 204/21	5′-ATATGCTTAARTTCAGCGGGT-3′	Van der Auwera *et al.* (1994)
28S	D2dnB	5′-CCTTGGTCCGTGTTTCAAGAC-3′	Kjer *et al.* (2001)
28S	R1411sq	5′-GTTGTTACACACTCCTTAGCGG-3′	Medina *et al.* (2001)
18S nucleomorph	Pyre_nm_F	5′-CAGTACGAACGATTTTGTACCGTG-3′	This study
18S nucleomorph	Pyre_nm_R	5′-AGGGACGTATTCAGCGCGAGT-3′	This study

separately analysed their nuclear- and nucleomorph-encoded ribosomal RNA genes in sets with 86 or 41 Pyrenomonadaceae strains obtained from the NCBI (National Center for Biotechnology Information) DNA nucleotide database (www.ncbi.nlm.nih.gov), respectively. *Proteomonas sulcata*, *Guillardia theta*, *Geminigera cryophila*, *Teleaulax amphioxeia* and *Falcomonas daucoides* were selected as outgroups due to their relatively close relationship with the Pyrenomonadaceae. Individual alignments of each gene were prepared with MAFFT online service (Katoh *et al.*, 2019). Ambiguously aligned regions were manually excluded in BioEdit (Hall, 1999). The nuclear 18S, 5.8S and 28S rRNA genes were then concatenated. Multiple sequence alignment of the nuclear-encoded rDNA operon (18S, ITS1, 5.8S, ITS2 and 28S rRNA) and the nucleomorph-encoded 18S rDNA are available in Supplementary Materials. Bayesian phylogenetic inference was performed using MrBayes 3.2.6 (Ronquist *et al.*, 2012) with four runs under the GTR+I+G4 model of evolution for 5 000 000 generations with 50% burn-in. Maximum likelihood (ML) phylogenetic inference was performed using IQ-TREE (Nguyen *et al.*, 2015) under the ModelFinder method (–m MFP) for model selection and 1000 bootstraps. The General Time Reversible with Invariant Sites and four discrete Gamma categories model (GTR+I+G4) was selected as the best model according to BIC and AIC. The phylogenetic trees were visualized using MEGA 6.0 (Tamura *et al.*, 2013). The GenBank accession numbers of the analysed sequences are given in the phylogenetic trees. Search for synapomorphies was performed using ancestral state reconstruction in IQ-TREE and the fixed ML phylogenetic tree. After calculating the ancestral states for each node of a given tree, we attributed apomorphic characters for some Pyrenomonadaceae clades. A character was considered apomorphic if it was reconstructed as ancestral for a taxon but not for the next deeper node on the tree. Genetic distances (uncorrected pairwise p-distance) between SSU and ITS rDNA sequences were calculated using MEGA 6.0 (Tamura *et al.*, 2013).

Secondary structure prediction

The secondary structures of nucleus-encoded ITS2 regions and helices 10 and 11 (Wuyts *et al.*, 2000) of 18S rRNA were predicted using the RNA folding software available at the mfold server (http://mfold.rna.albany.edu/?q=mfold/RNAFolding–Form) (Zuker, 2003) with default parameters. All predicted ITS2 structures were manually examined and compared for common stems, loops and bulges. Compensatory base changes (CBCs) in helices were manually identified from the ITS2 secondary structures.

Results and discussion

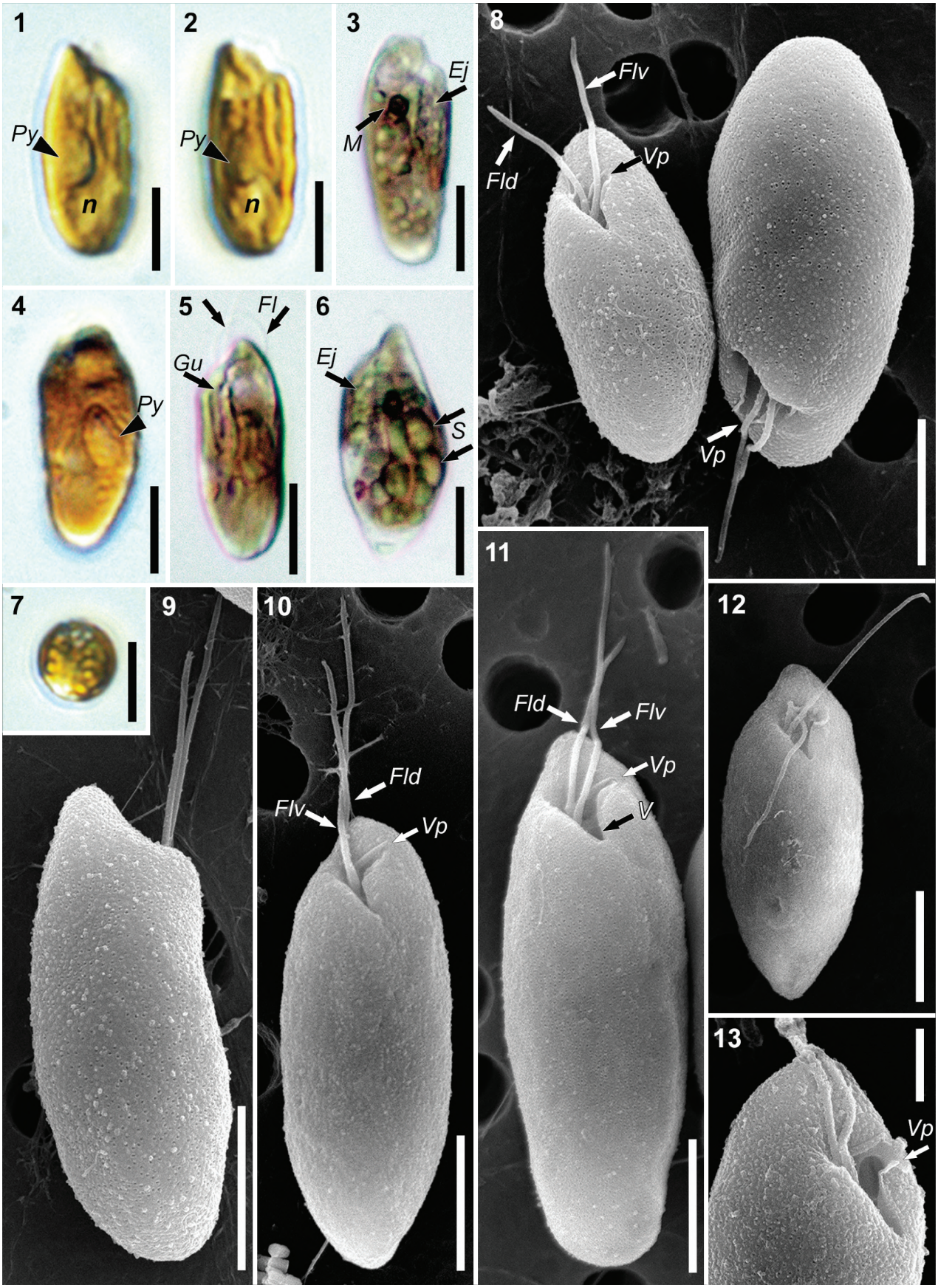
Morphology of novel cryptophyte strains from the Black Sea

Morphological observations of strain IBSS-Cr-7S4

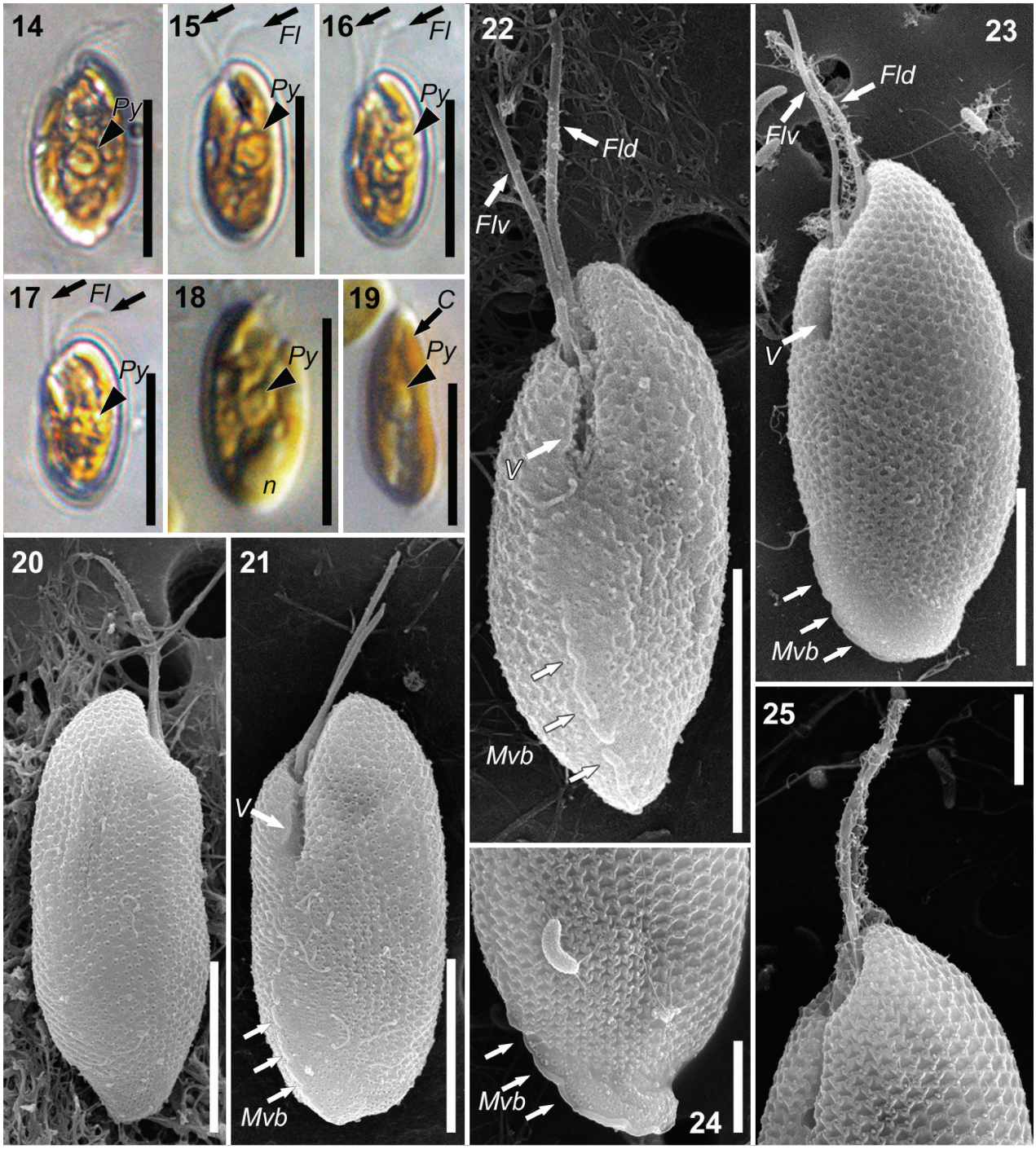
Live motile cells of strain IBSS-Cr-7S4 were mainly elongated and fusiform in dorsal or ventral views (Figs 1–6, 8–12), with slight dorso-ventral compression. The apex and, frequently, the antapex were narrowed towards the extremities. When viewed laterally, the cell apex appeared slightly rhinose (Figs 1, 2, 5, 6, 9). Measurements of live motile cells under LM (×600) ranged 19–27.4 μm in length (mean 25.2 ± 2.1 μm, median = 22.5, n = 20) and 8.9–12.5 μm in width (mean 10.2 ± 1.3 μm, median = 10.0, n = 20). Corresponding measurements under SEM (×3000) were 11.8–20.3 μm in length (16.0 ± 2.0 μm, n = 20) and 4.9–7.6 μm in width (6.1 ± 0.7 μm, n = 20). A single, vertically elongated pyrenoid with an irregularly bevelled shape was positioned dorsally between the two lobes of the chloroplast (Figs 1, 2, 4). The nucleus was located in the posterior half of the cell (Figs 1, 2). SEM observations revealed the presence of two unequal, relatively long flagella. The ventral flagellum was approximately 3/4 of the cell length and slightly longer than the dorsal one, which reached ~2/3 the length of the ventral flagellum (Figs 8–12). The flagella were inserted into an open, subapical, triangular and short (~1/5 cell length) vestibulum (Figs 8, 11). The narrow vestibular plate was semi-tubular and depressed on the left side of the vestibulum (Figs 8, 10, 11, 13). The inner periplast component (IPC) consisted of a continuous, sheet-like, papillate layer, with numerous small underlying ejectosomes (Figs 8, 9, 13). Motile cells frequently exhibited changes in direction, swimming forward at relatively low speed, and rotating around their anterior-posterior axis. A notable swarming effect was observed under LM illumination. In ageing cultures, non-motile cells were common, forming a bottom layer and exhibited considerable variation in shape and size.

Morphological observations of strain IBSS-Cr-4.2.G

Live motile cells of strain IBSS-Cr-4.2.G were elongated, with a convex dorsal surface and mostly flat ventral margin (Figs 14–18, 20, 21, 23). In lateral view, the apex appeared obliquely truncate due to the orientation of the vestibulum-furrow complex (Figs 14, 18, 20–22, 25). Mature cells were strongly dorso-ventrally compressed and frequently twisted along the longitudinal axis, with the apex deflected to the right and the antapex to the left. In dorsal or ventral view, the antapex was rounded, while the apex was truncated obliquely from the top to 1/3 of the cell height. Live cells measured under LM (×600) were



Figs 1–13. *Eomonas fusiformis* sp. nov., diplomorph (strain IBSS-Cr-7S4). **Figs 1–3**. Right lateral view showing pyrenoid (Py), nucleus (n) in the posterior part of the cell, Maupas ovals (M) and large ejectosomes (Ej) lining the gullet. **Figs 4–6**. Left lateral view showing pyrenoid (Py), ejectosomes (Ej), flagella (Fl), gullet (Gu) and starch granules (S). **Fig. 7**. Resting cyst with a thick cell wall from an old culture. **Fig. 8**. Two cells in ventral (left cell) and ventro-lateral (right cell) views showing size variability, dorsal (Fld) and ventral (Flv) flagella, and vestibulum plates (Vp). **Fig. 9**. Right lateral view showing two unequal flagella. **Figs 10–12**. Ventral view showing a short V-shaped vestibulum (V) with a concave vestibulum plate (Vp) depressed on the right side, the ventral flagellum often fits into this depression. **Fig. 13**. Detailed view of the apex, showing the vestibulum with vestibulum plate (Vp). Figs 1–7, LM; Figs 8–13, SEM; scale bars: Figs 1–7, 10 μm; Figs 8–12, 5 μm; Fig. 13, 2 μm.



Figs 14–25. *Eomonas vitalis* sp. nov., haplomorph (strain IBSS-Cr-4.2G). **Figs 14–17**. Left lateral view showing a large central pyrenoid (Py) and flagella (Fl). **Figs 18, 19**. Right lateral view showing pyrenoid (Py), chloroplast (C) and posterior nucleus (n). **Fig 20**. Right lateral view. **Figs 21–23**. Ventro-lateral (Figs 21, 23) and ventral (Fig. 22) views showing a short V-shaped vestibulum (V), dorsal (Fld) and ventral (Flv) flagella, and mid-ventral band (Mvb, arrows). **Fig. 24**. Detailed antapex in ventral view showing mid-ventral band (Mvb, arrows). **Fig. 25**. Detailed apex in ventro-lateral view. Figs 14–19, LM; Figs 20–25, SEM; scale bars: Figs 14–19, 10 µm; Figs 20–23, 5 µm; Figs 24, 25, 2 µm.

15–22.5 µm in length (mean 18.6 ± 2.6 µm, median = 17.5, n = 20) and 7.5–13.8 µm in width (mean 9.9 ± 0.7 µm, median = 10.0, n = 20). Corresponding measurements under SEM (×1500–8000) were 13.4–18.6 µm in length (16.8 ± 2.0 µm, n = 20) and 4.9–6.8 µm in width (7.3 ± 3.7 µm, n = 20). A single parietal, bilobed chloroplast occupied the entire dorsal margin and extended across half of the ventral margin (Figs 14–19). A single rounded pyrenoid was located centrally between the two chloroplast lobes (Figs 14–19). The nucleus was visible in the posterior half of the cell near the rounded antapex (Fig. 18). LM and SEM observations revealed two subequal flagella (Figs 14–17, 20–23), with the dorsal flagellum being slightly longer than the ventral, at ~1/2 of the cell length, inserted into a vestibulum (Figs 21–23, 25). A short, closed vestibulum continues with an elongated furrow, extending up to 1/3 of the cell

length from the apex (Figs 21–23, 25). A mid-ventral band extended from the antapex up to 1/2 of the cell length (Figs 21–24). The inner periplast component composed of an ordered system of discrete, stepped plates, exhibited a superficial honeycomb-like pattern of regular hexagons in whole-mounted SEM cells (Figs 20–25). In older cells, these plates were largely absent at the antapex, where they were replaced by a sheet-like structure (Figs 22–24), with remnants of the mid-ventral band often appearing as a flounce-like, sheet-like IPC with distinct small pores remaining from discharged ejectosomes (Fig. 24). Longitudinal sections of the cell show the pyrenoid surrounded by a starch sheath at the cell centre between two lobes of the chloroplast. The nucleomorph is embedded within an axial groove into the pyrenoid and enclosed by a double membrane (Figs 38, 39). Motile cells typically moved forward at low speed with characteristic shuttle-like movements, often oriented vertically, 'on the side' – with the plane perpendicular to the surface and tilted at an angle to it, with the apex pointing downward. The cells also rotated slowly around the anterior–posterior axis. Live but sluggish cells formed conglomerates on a matrix of ejectosomes at the bottom of the vessel. No cysts or palmeloid forms were observed.

Morphological observations of strain IBSS-Cr-4.19

The live motile cells of strain IBSS-Cr-4.19 were oblong-ovate to elliptical in dorsal or ventral views, with a length-to-width ratio of 2.5 ± 0.5 (Figs 26–29). The cells were dorso-ventrally compressed, with a width-to-depth ratio of about 2–3 (Figs 32–36). Measurements of live cells under LM (×600) ranged 14.1–20.1 µm in length (mean 16.7 ± 2.2 µm, median = 16.5, n = 20) and 7.1–12.8 µm in width (mean 8.8 ± 2.3 µm, median = 8.0, n = 20). Corresponding measurements under SEM (×3000–8000) were 11.2–19.0 µm in length (mean 14.7 ± 2.5 µm, n = 20) and 4.9–7.7 µm in width (mean 5.9 ± 0.8 µm, n = 20). In ventral and dorsal views, both the apex and antapex appear rounded (Figs 32–36), while the apex was rhinose in lateral view (Figs 26–28, 30, 31, 34, 37). The gullet was lined with rows of large ejectosomes (Fig. 31). The nucleus was located in the posterior half of the cell (Figs 26, 31). A single light-brown, H-shaped, parietal chloroplast extended from the apex to the antapex (Figs 26–32). A round, brown pyrenoid was distinctly visible at LM and located centrally between the chloroplast lobes (Figs 26–30). Two unequal flagella emerged from the base of a short (approximately 1/6 of the cell length), deep, V-shaped, subapical vestibulum, that is slightly bevelled to the left and possessed a vestibular plate on its left side (Figs 32, 34–37). The ventral flagellum was slightly longer than the dorsal one, the latter was approximately 1/3 of the cell length (Figs 34–37). The vestibular plate formed a semi-tubular depression on the right side into which the ventral flagellum fits (Figs 36, 37). The inner periplast component was a continuous, sheet-like and papillate layer (Figs 34–37), with numerous small underlying ejectosomes. Pores remained visible following the discharge of ejectosomes (Fig. 37). The mid-ventral band was absent. In a longitudinal section of the cell, the nucleomorph was embedded within an axial groove into the pyrenoid and enclosed by a double membrane (Fig. 40). In a drop of a live culture placed on a glass slide under LM, the cells exhibited a coordinated swarming effect, moving towards the centre of the drop regardless of the illumination intensity. This swarming behaviour was triggered within seconds of light stimulation and attained saturation within 30s. If the drop was disturbed, multiple secondary concentration centres (3–5) typically formed within the same period of time (~30 seconds).

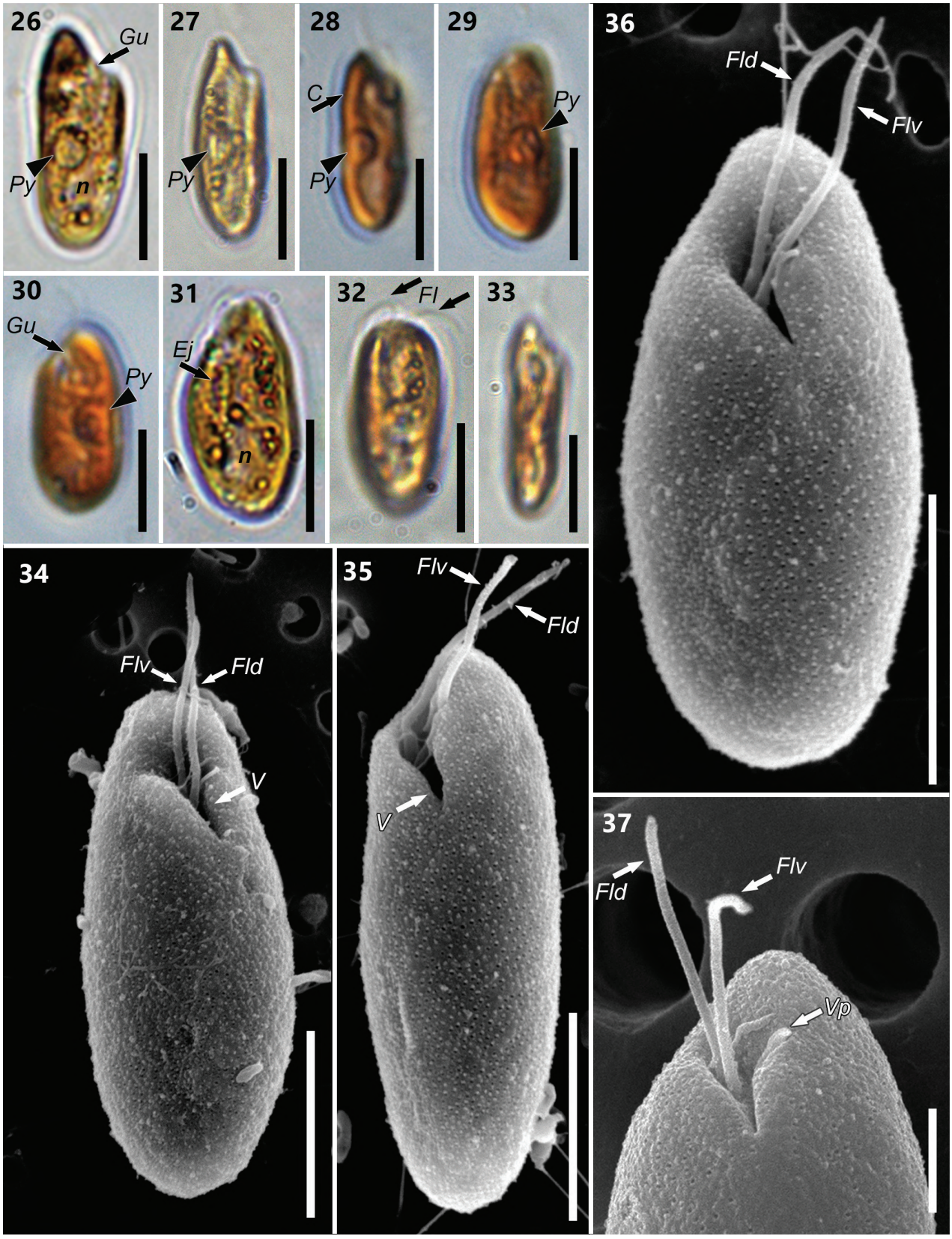
Pigment analysis

Dense clonal cultures of the strains IBSS-Cr-4.19, IBSS-Cr-4.2G and IBSS-Cr-7S4 with cell concentrations higher than 10^4 cells ml^{-1} exhibited characteristic red-brick colouration towards the end of exponential growth phases (Supplementary fig. S1). Phycobiliprotein extracts showed nearly identical spectral profiles (Fig. 41). The absorption spectra were characterized by a light-harvesting peak at 545 nm, indicative of phycoerythrin 545 (PE-545), and a secondary chlorophyll-related peak at 675 nm.

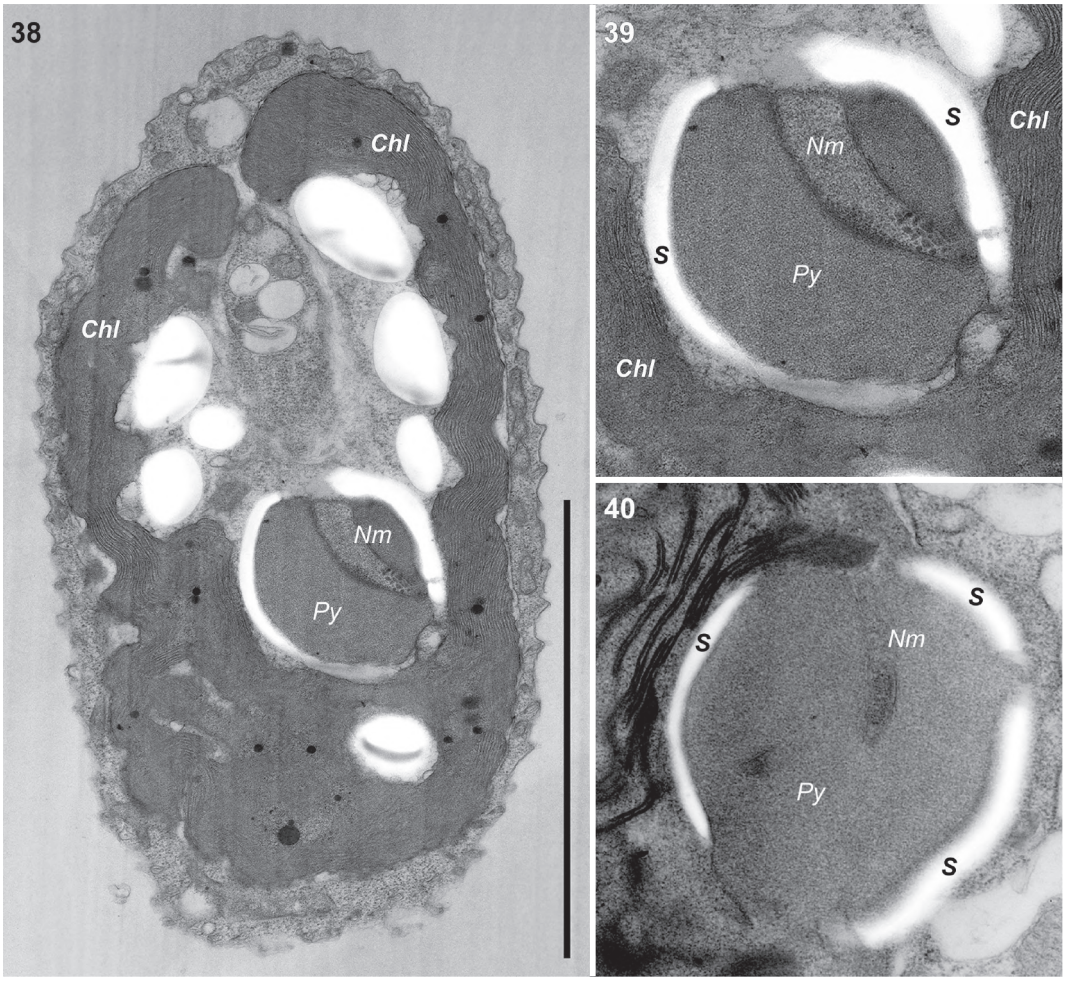
Morphological consideration

The SEM-defined morphological characteristics of strains IBSS-Cr-7S4 and IBSS-Cr-4.19 were notably similar. Both possess a sheet-like IPC, a comparable vestibulum and vestibular plate structure, and both lack a mid-ventral band. However, these strains can be clearly distinguished in live cultures under LM by their distinct cell shapes, dimensions and pyrenoid features. Cells of strains IBSS-Cr-7S4 are longer, fusiform, with more acute apex, and a rounded pyrenoid compared to a more rounded, ovoid cell of IBSS-Cr-4.19 with an irregularly bevelled pyrenoid. Conversely, strains IBSS-Cr-4.19 and IBSS-Cr-7S4 both differ significantly in morphology when compared to IBSS-Cr-4.2G. Cells of the latter possess a plated IPC, a true furrow and a prominent mid-ventral band.

Comparison of newly isolated cryptophyte strains with historical taxonomic records from Sevastopol Bay, Black Sea (Rouchijajnen, 1967, 1970) remains constrained by the brevity of the original descriptions and illustrations, which lack ultrastructural detail. Strains IBSS-Cr-4.19 and IBSS-Cr-7S4 bear a resemblance to



Figs 26–37. *Eomonas vitalis* sp. nov., diplomorph (strain IBSS-Cr-4.19). **Figs 26–28**. Right lateral view showing pyrenoid (Py), gullet (Gu) and chloroplast (C). **Figs 29–31**. Left lateral view showing pyrenoid (Py), nucleus (n), gullet (Gu) and ejectosomes (Ej). **Figs 32, 33**. Ventral view showing flagella (Fl). **Fig. 34**. Ventro-lateral view showing dorsal (Fld) and ventral (Flv) flagella and vestibulum (V). **Figs 35, 36**. Ventral view showing dorsal (Fld) and ventral (Flv) flagella and vestibulum (V). **Fig. 37**. Detailed apex in ventral view showing dorsal (Fld) and ventral (Flv) flagella emerging from a short V-shaped, bevelled vestibulum (V) with a semi-tubular vestibulum plate (Vp) depressed on the left side. Figs 26–33, LM; Figs 34–37, SEM; scale bars: Figs 26–33, 10 μm; Figs 34–36, 5 μm; Fig. 37, 2 μm.



Figs 38–40. Ultrastructure of cells in *Eomonas vitalis* sp. nov., strain IBSS-Cr-4.2G, haplomorph (38, 39) and IBSS-Cr-4.19, diplomorph (40), visualized with transmission electron microscope (TEM). **Fig. 38**. Longitudinal section of a cell through the pyrenoid (Py) and the embedded nucleomorph (Nm), chloroplast (Chl) is seen. **Figs 39, 40**. Part of transverse section, showing detail of a starch (S) sheathed pyrenoid (Py) region, the embedded nucleomorph (Nm) is seen. Scale bar: **Fig. 38**, 5 μm.

the recently described from the Black Sea *Rhodomonas storeatuloformis* (Khanaychenko *et al.*, 2022) in terms of cell shape, the structure of the vestibulum and the type of the inner periplast component. However, cells of strain IBSS-Cr-7S4 were larger: 19–27.4 × 8.9–12.5 μm vs. 12–19 × 5–10 μm in *R. storeatuloformis*. Although the size of IBSS-Cr-4.19 overlaps with *R. storeatuloformis*, it can be distinguished by its rounded antapex, which contrasts with the tapered and slightly curved posterior end of the latter. Despite the minor morphological differences between IBSS-Cr-4.19 and *R. storeatuloformis*, the two taxa are only distantly related phylogenetically (Fig. 42). Given the lack of extant type material or molecular data for historical taxa isolated from the same area, the strains examined here are described as new species to ensure taxonomic stability.

Applying traditional genus-level criteria, strains IBSS-Cr-7S4 and IBSS-Cr-4.19 characterized by a non-plated sheet-like IPC, the absence of true furrow and mid-ventral band would be assigned to the genus *Storeatula*. Conversely, strain IBSS-Cr-4.2G, with its superficial hexagonal pattern would be placed in *Rhinomonas*, yet the presence of a true furrow and mid-ventral band suggests its affinity to *Rhodomonas*. This systematic inconsistency is a long-recognized issue within the Pyrenomonadaceae (Deane *et al.*, 2002; Hoef-Emden *et al.*, 2002; Lane *et al.*, 2005; Shalchian-Tabrizi *et al.*, 2008; Cunningham *et al.*, 2019; Daugbjerg & Devantier, 2024), underscoring the inability to resolve the taxonomy of this group through morphological observation alone. The reliance on phenotypic markers, which are now recognized as being highly plastic or life-cycle dependent, has resulted in the paraphyly of established genera and the marked incongruence between morphological and molecular datasets. Consequently, robust taxonomic resolution necessitates the prioritization of molecular data, which provides the stable phylogenetic framework required to reconcile these structural disparities and define natural evolutionary lineages.

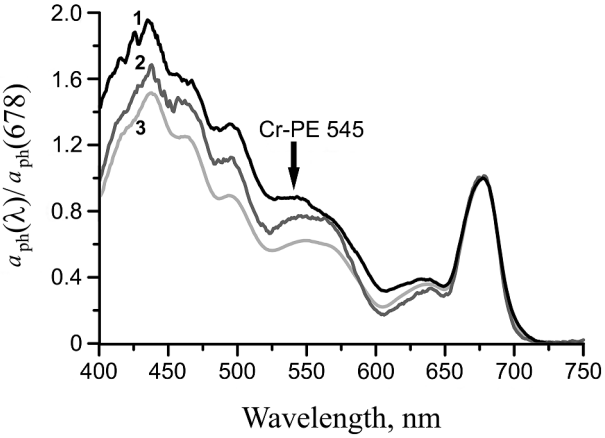


Fig. 41. Absorption spectra normalized at 678 nm ($a_{ph}(\lambda)/a_{ph}(678)$) of *Eomonas fusiformis* sp. nov. (1, strain IBSS-Cr-7S4) and *Eomonas vitalis* sp. nov. (2, strain IBSS-Cr-4.2G and 3, strain IBSS-Cr-4.19). The arrow indicates a peak of phycoerythrin Cr-PE-545.

Concordance between morphological and molecular datasets in the Pyrenomonadaceae

In order to assess the concordance between morphological and molecular datasets within the Pyrenomonadaceae, an extensive search was performed to integrate species descriptions with available genetic information. Data were extracted from the extensive taxonomic literature to summarize the current knowledge on species morphology, with a specific focus on strain designation and geographic origin to establish a robust link between described taxa, extant culture collections accessions and nucleotide sequences in public databases (e.g. GenBank). By tracking species synonymy, original and subsequent strain designations, and associated metadata, we assessed a total of 31 currently recognized taxa classified in the Pyrenomonadaceae. The related data for each taxon are summarized in Supplementary table S1, which serves as a baseline for assessing the detail and sufficiency of the morphological and molecular descriptions currently available for each species.

Our survey of matching morphological and molecular datasets revealed 16 of the reviewed taxa lacking corresponding genetic sequences. Many of these are uncultured species described between the late 19th and mid-20th centuries, pre-dating the advent of molecular phylogenetics (*Rhodomonas gracilis* J.Schiller 1926; *Rhodomonas pelagica* Lohmann 1908; *Rhodomonas pusilla* (H.Bachmann) Javornický 1967; *Rhodomonas rubra* Geitler 1922; *Rhodomonas ruttneri* J.Schiller 1926; and *Rhodomonas tenuis* Skuja 1948; Supplementary table S1). The original descriptions of these taxa are frequently ambiguous, with illustrations constrained by the optical limitations of the period, and type materials are often lost or were never designated. Moreover, emending these historical descriptions to incorporate molecular data and designate epitypes to stabilize their identity is exceptionally challenging, if not impossible. The lack of DNA suitable for sequencing and the scarcity of diagnostic characters in the original descriptions often preclude a definitive link between historical species names and newly isolated taxa.

A second subset included taxa transferred to *Rhodomonas* or *Rhinomonas* during subsequent taxonomic revisions based solely on historical descriptions, without the provision of additional morphological data (*Rhodomonas heteromorpha* Butcher *ex* Hill & Wetherbee 1989; *Rhinomonas fragarioides* (Butcher) D.R.A.Hill & R.Wetherbee 1988; *Rhinomonas fulva* (Butcher) D.R.A.Hill & R.Wetherbee 1988; and *Rhinomonas lateralis* (Butcher) D.R.A.Hill & R.Wetherbee 1988; Supplementary table S1).

The third subset comprised taxa for which morphological descriptions are comprehensive, incorporating examination of external (LM, SEM) and internal (TEM) morphology, as well as pigment analysis to show key diagnostic characters (*Rhodomonas stigmatica* (Wisłouch) D.R.A.Hill 1991; *Rhodomonas ovalis* Nygaard 1949; *Rhinomonas reticulata* (Lucas) Novarino var. *compressa* Novarino 1991; and *Storeatula rhinosa* P.Kugrens, B.L.Clay & R.E.Lee 1999; Supplementary table S1). While authentic strains for these taxa are maintained in either public or private culture collections, the available strains have not yet been subjected to molecular analysis. Overall, the inability to integrate the above-listed 16 taxa into molecular phylogenies results in nearly half of the family's known morphospecies being overlooked in modern evolutionary frameworks, hindering the interpretation of evolutionary relationships within the family.

Conversely, a more taxonomically stable group exists where detailed morphological descriptions are directly linked to molecular data. This group primarily consists of recently described species with available type or authentic strains and older taxa that have been reassessed through modern morphological and genetic analyses based on original type strains. The following 13 taxa are included: *Rhodomonas abbreviata* (Butcher) D.R.A.Hill & R.Wetherbee 1989, strain CCAP 976/16; *Rhodomonas chrysoidea* Butcher *ex* D.R.A.Hill & R.Wetherbee 1989, strain NIES701; *Rhodomonas falcata* Butcher *ex* Hill & Wetherbee 1989, strain NIES702; *Rhodomonas irregularis* Butcher *ex* Erata & Chihara 1989, strain NIES698; *Rhodomonas maculata* Butcher *ex* Hill & Wetherbee 1989, strain CCAP 979/14; *Rhodomonas marina* (Dangeard, 1892) Lemmermann 1903 *emend.* Daugbjerg & Devantier 2024, strain S18, epitype; *Rhodomonas salina* (Wisłouch) D.R.A.Hill & R.Wetherbee 1989, strain CCAP 978/24; *Rhodomonas storeatuloformis* Khanaychenko,

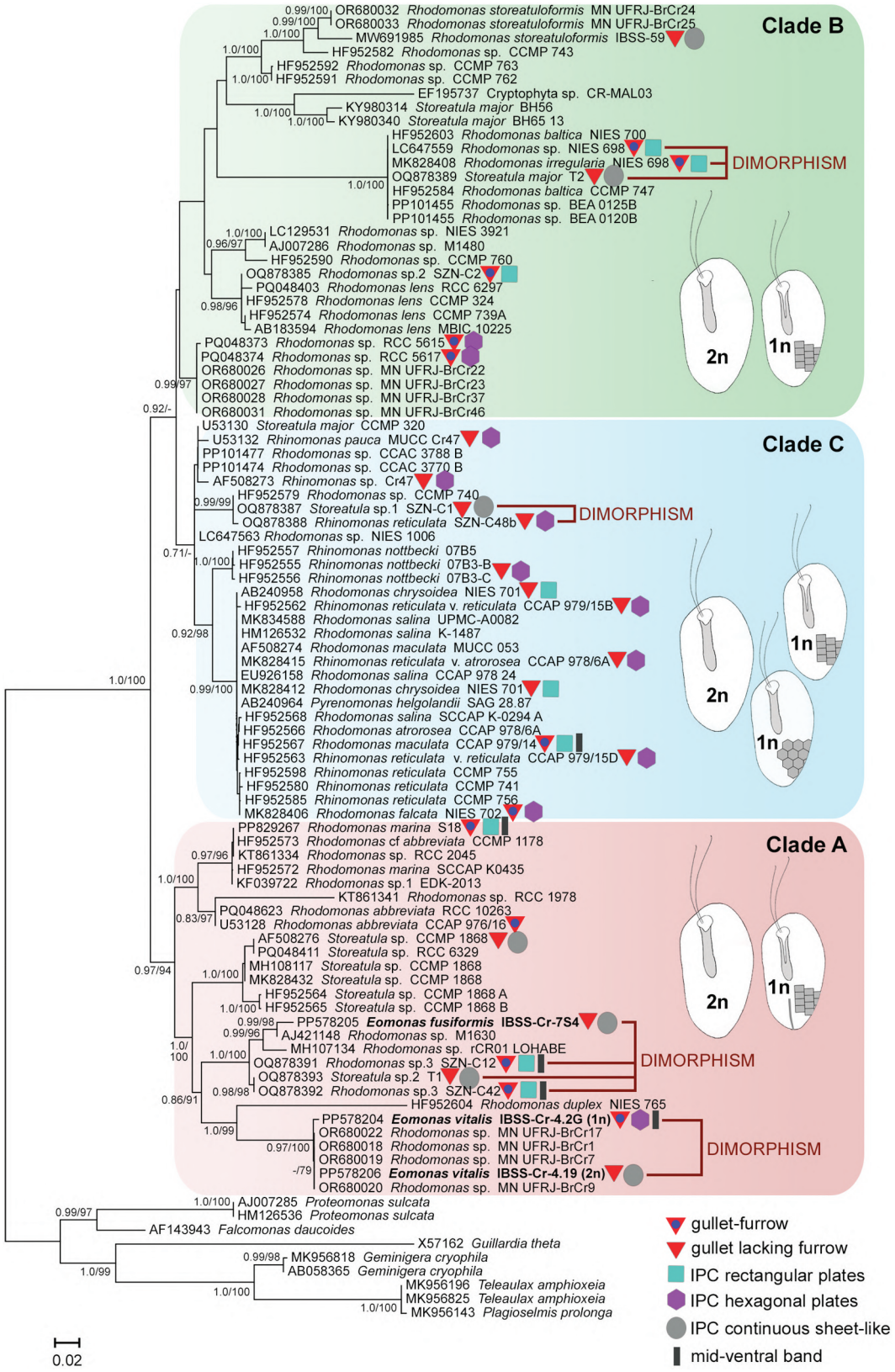


Fig. 42. Bayesian phylogenetic tree based on concatenated nuclear-encoded 18S, ITS/5.8S and 28S rRNA gene sequences of the family Pyrenomonadaceae. Posterior probabilities (left) and maximum likelihood bootstrap support values (right) are shown at the nodes. Parameter values which are lower than 0.7 or 70% are unlabelled. Clade names follow Majaneva *et al.* (2014). GenBank accession numbers are given to the left and the strain numbers to the right of the strain name. Novel cryptophyte strains are highlighted (in bold) in Clade A.

Saburova, Aleoshin, Rylkova, O.V.Popova & Aganesova 2022, strain IBSS–59; *Rhinomonas nottbeckii* J.-M.Rintala, M.Majaneva, I.Remonen & Blomster 2014, strain 07B3; *Rhinomonas pauca* D.R.A.Hill & Wetherbee 1988, strain MUCC Cr47; *Rhinomonas reticulata* (I.A.N. Lucas) G.Novarino 1991, strain CCAP 979/15; *Rhinomonas reticulata* var. *atrorosea* (Butcher *ex* D.R.A.Hill & R.Wetherbee) G.Novarino 1991, strains NIES699, CCAP 978/6A and CCAP 978/6B (refer to Supplementary table S1 for strain details).

Additional morphological data were gathered from relevant taxonomic surveys of cryptophyte diversity. Strains of *Rhodomonas* spp., *Rhinomonas* spp. and *Storeatula* spp. were described, illustrated and sequenced from the Mediterranean Sea, Italy (Cerino & Zingone, 2006) and Brazilian coastal lagoons (Magalhães, 2018). Furthermore, the present study supplements this group with three newly isolated Black Sea strains, further bridging the gap between phenotypic and genotypic data.

Finally, four taxa remain in a state of taxonomic uncertainty: they are well-described morphologically but lack molecular data directly linked to type specimens or recently verified strains, including *Rhodomonas baltica* Karsten 1898, *Rhodomonas duplex* D.R.A.Hill & R.Wetherbee 1989, *Rhodomonas lens* Pascher & Ruttner 1913, and *Storeatula major* D.R.A.Hill 1991 (Supplementary table S1). The lack of consolidated data for *Rhodomonas baltica* and *Storeatula major* is particularly concerning, as both are generitypes. The existing gap in molecular data for these nomenclatural types continues to represent a significant challenge, as it hinders the delineation of precise generic boundaries within the Pyrenomonadaceae, thereby contributing to systematic instability.

Molecular phylogeny

Phylogenies inferred from nuclear and nucleomorph (nmSSU) data generally had congruent topologies in BI and ML analyses. In the combined tree (Fig. 42), internal branches were better resolved and received higher statistical support than in single-gene phylogenies (Supplementary figs S2–S4).

All Pyrenomonadaceae strains clustered into a monophyletic group in both the nuclear- and nucleomorph-based phylogenetic trees (Fig. 42 and Supplementary figs S2–S4), with posterior probability/maximum likelihood bootstrap support values of 1.0/100 and 0.75/73, respectively. The Pyrenomonadaceae clade was further split into two large sister clades, of which one clade can be subdivided into two subclades, albeit poorly resolved. The resulting branching pattern is consistent with Clades A, B and C, previously identified among Pyrenomonadaceae (Majaneva *et al.*, 2014).

A weakly supported Clade B comprised strains assigned to *Rhodomonas* and *Storeatula*, namely *R. baltica*, *R. storeatuloformis*, *R. irregularis*, *R. lens* and *S. major*. A number of unidentified *Rhodomonas* strains either clustered with taxonomically recognized species or formed independent lineages, likely representing as-yet-undescribed species (e.g. *Rhodomonas* sp. strains RCC5615, RCC5617, MN UFRJ-BrCr22, MN UFRJ-BrCr23, MN UFRJ-BrCr37 and MN UFRJ-BrCr46). Notably, a set of genetically identical strains was grouped within a single clade, including *Rhodomonas irregularis* (NIES 698), *Storeatula major* (T2) and the generitype *Rhodomonas baltica* (NIES700 and CCMP747), reflecting the current taxonomic uncertainty within the genus *Rhodomonas*.

Clade C similarly contained intermingled strains of *Rhodomonas*, *Storeatula* and *Rhinomonas*, further reinforcing the paraphyly of these genera. Within this clade, the precise placement of the type species (*Rhinomonas pauca* MUCC Cr47) across *Rhodomonas* and *Storeatula* strains remained unresolved due to low branch support. Conversely, all *Rhinomonas nottbecki* strains formed a distinct, full-supported lineage. Several *Rhinomonas reticulata* strains (SZN-C48b, CCAP 979/15, CCMP741, CCMP755 and CCMP756) were nested within distant subclades alongside *Rhodomonas* spp.

A notable topological feature was a highly supported subclade (0.99/100) within Clade C, resolved as sister to the *Rhinomonas nottbeckii* branch. This lineage encompassed strains with nearly identical SSU and ITS rDNA sequences yet was assigned to six distinct species (*Rhodomonas chrysoidea*, *R. salina*, *R. maculata*, *R. falcata*, *Rhinomonas reticulata* & var. and *Pyrenomonas helgolandii*) (Fig. 42). The negligible genetic divergence within this cluster suggests that these disparate morphotypes may represent a single taxon, rendering their current generic and species-level boundaries uncertain. Such a collapse of multiple taxa into a single lineage underscores the limitation of conventional diagnostic criteria and necessitates a thorough taxonomic revision to reconcile phenotypic plasticity with evolutionary history.

Clade A was clearly distinct from a sister B + C cluster with high support (0.97/94). This clade grouped three taxonomically recognized species, namely *Rhodomonas marina*, *R. abbreviata* and *R. duplex*, along with a number of unidentified strains of *Rhodomonas* and *Storeatula*. All three novel isolates from the Black Sea described in this study were nested within Clade A as well (Fig. 42).

The fully supported branch was anchored by the authentic *Rhodomonas marina* strain S18 (Daugbjerg & Devantier, 2024) and further included several unidentified *Rhodomonas* strains and the likely misidentified *Rhodomonas* cf. *abbreviata* CCMP1178. The

high genetic similarity of these strains to epitype (strain S18) suggests their taxonomic identity with *Rhodomonas marina* sensu Daugbjerg & Devantier (2024). This clade formed the closest sister group to *Rhodomonas abbreviata* lineage. Closely related strains of *Storeatula* sp. (CCMP1868 and its subcultures) were grouped into a well-supported subclade, while exhibiting somewhat intrastrain genetic variability among subclonal cultures.

Novel strain IBSS-Cr-7S4 formed a distinct cluster (0.99/96) with two unidentified *Rhodomonas* strains, exhibiting small genetic distances to its closest sister clade comprising *Rhodomonas* and *Storeatula* strains (p-distance = 0–0.7% on the SSU rDNA level among all strains; Supplementary table S2).

The two other novel isolates, IBSS-Cr-4.2G and IBSS-Cr-4.19, clustered with four unidentified *Rhodomonas* strains from Brazil into a fully supported clade (1.0/100) with negligible interstrain divergence (p-distance 0–0.1%; Supplementary table S2). This clade was resolved as a sister group to *Rhodomonas duplex*.

The results presented herein are consistent with recent phylogenetic findings (Marin *et al.*, 1998; Deane *et al.*, 2002; Shalchian-Tabrizi *et al.*, 2008; Majaneva *et al.*, 2014; Khanaychenko *et al.*, 2022; Solarska *et al.*, 2023; Daugbjerg & Devantier, 2024; Hoef-Emden *et al.*, 2024), confirming that the genera *Rhodomonas*, *Rhinomonas* and *Storeatula*, as currently circumscribed, are not monophyletic and instead form weakly supported intermixed clades. The recurring paraphyly of these genera across various phylogenetic studies and multiple genetic markers, coupled with genotypic identity across disparate taxa (e.g. Marin *et al.*, 1998; Deane *et al.*, 2002; Daugbjerg & Devantier, 2024; this study), underscores the necessity for taxonomic revision within the Pyrenomonadaceae, as proposed in this study.

Molecular signatures

The robust support for Clade A and its clear phylogenetic divergence from Clades B + C suggest that specific molecular markers define these major lineages. We identified diagnostic characters with low to moderate variability within each lineage and evaluated these molecular signatures to determine whether they represent synapomorphies or symplesiomorphies and whether they are suitable for distinguishing between these two species groups.

In the nuclear-encoded 18S rRNA, the loop of variable helix 10 (numbered according to Wuyts *et al.*, 2000) in Clade B + C strains matched the outgroup (symplesiomorphy), whereas in Clade A strains it either acquired a specific motif or was entirely lost (Fig. 43). Conversely, the loop of variable helix 11 in Clade A strains matched the outgroup, while Clade B + C strains were distinguished by an apomorphic motif (Fig. 44). Similar patterns were observed in the 5.8S rRNA gene sequences, where Clade A retained a plesiomorphic state and Clade B + C exhibited a distinct apomorphy (Fig. 45).

The analysis of the nucleomorph-encoded 18S rRNA further reinforced this separation, providing three additional diagnostic signatures that distinguish Clade A from Clade B + C. A key generic synapomorphy was identified where Clade A strains possessed the motif 5'-**C**-TRGCGGCRGCG-3', contrasting with the symplesiomorphic motif 5'-**T**-TGGYGGCRGCG-3' found in Clade B + C strains (synapomorphic characters are bolded). Furthermore, a site-specific substitution within a conserved motif differentiates the two Pyrenomonadaceae lineages, with 5'-GCTCGTAGTCGAAT-**C**-3' in Clade A versus 5'-GCTCGTAGTCGAAT-**T**-3' in Clade B + C. A third signature is located within a conserved flanking motif 5'-GCGTGAGTCAT-**X**-AACTCGCG CT-3', where the variable position (X) is occupied by cytosine (C) in Clade A strains and thymine (T) in Clade B + C strains.

These findings confirm a deep basal divergence within the Pyrenomonadaceae, allowing each major clade to be characterized by a unique set of molecular signatures. The identified stable markers provide a robust multi-genome diagnosis regardless of morphological variability. Therefore, we established *Eomonas* gen. nov. for the species of Clade A, while the species of Clade B + C, including the type species *Rhodomonas baltica*, are herein retained within a redefined '*Rhodomonas* complex'.

While *Eomonas* gen. nov. and *Rhodomonas* complex exhibited similar sets of morphotypes, making them nearly indistinguishable under light and electron microscopy, our multi-locus phylogenetic analysis revealed a notable genetic divergence that warrants generic separation. The two main lineages within Pyrenomonadaceae are delineated by specific molecular signatures within the nuclear and nucleomorph genomes. Such 'cryptic' generic differentiation is increasingly recognized in the Cryptophyceae, where morphological evolution often lags behind genomic divergence (e.g. Hoef-Emden, 2007; Majaneva *et al.*, 2014; Gusev *et al.*, 2022). By defining *Eomonas* through these stable molecular synapomorphies, we ensure that the taxonomic classification reflects the true evolutionary history of the Pyrenomonadaceae, rather than relying on homoplasious morphological traits.

The interpretation of genetic distances in the Cryptophyceae is often complicated by significantly differing evolutionary rates among lineages. For instance, the genus *Cryptomonas* is known for its accelerated substitution rates within the ribosomal operon compared to more conservative clades (Hoef-Emden, 2007; Gusev *et al.*, 2022). In the phylogenetic

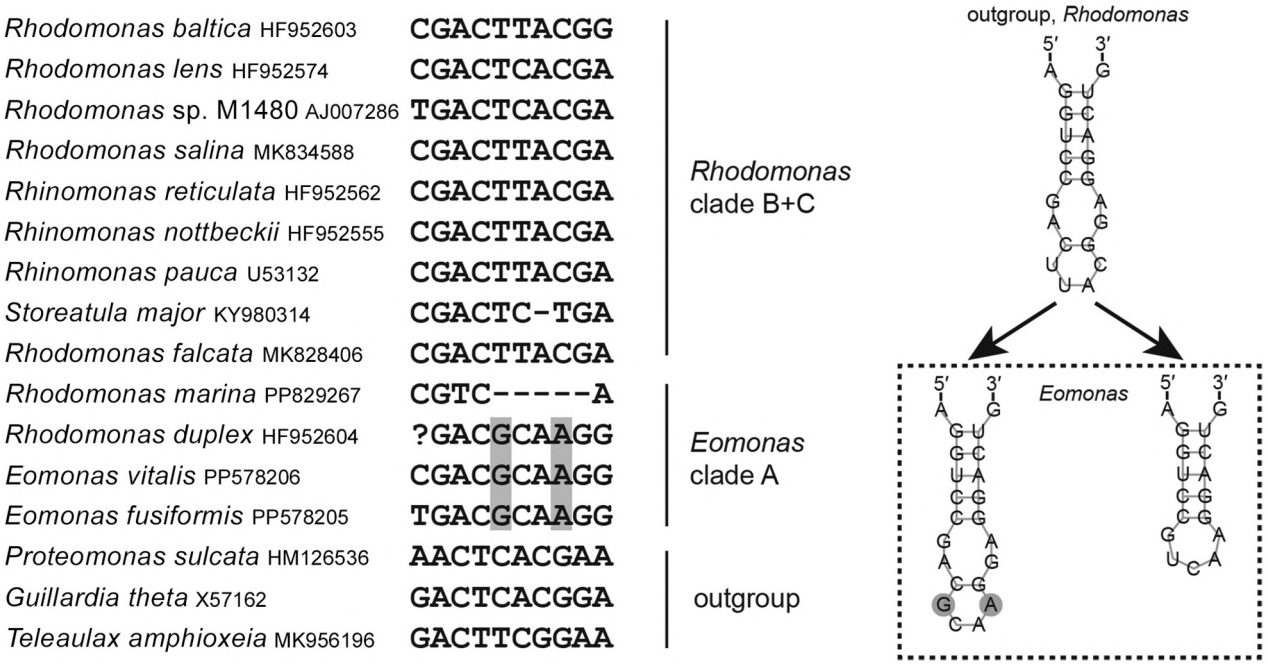


Fig. 43. Molecular diagnosis of *Eomonas* gen. nov. Left: alignment of hairpin 10 of SSU rRNA. Right: predicted secondary structures of hairpin 10 of SSU rRNA for the genus *Rhodomonas*, which retains the plesiomorphic structure, and two structural variants for the genus *Eomonas*. Synapomorphic nucleotides for the genus *Eomonas* are highlighted in grey.

tree of the Pyrenomonadaceae, the branches appeared shorter than those typically observed in the Cryptomonadaceae, suggesting either a slower evolutionary rate within the family or a younger geological age of the extant lineages. However, the high degree of congruence between our nuclear and nucleomorph datasets indicates that the recovered topology is robust and unlikely to be an artefact of rate heterogeneity. While the genetic distances separating the genera within the Pyrenomonadaceae may be smaller in scale, they define stable phylogenetic lineages. Thus, the recognition of these generic boundaries is justified by molecular evidence.

Predicted secondary structures of nuclear ITS2 regions

Compensatory base substitutions (CBCs) in the ITS2 region are widely regarded as a reliable criterion for verifying the species boundaries in algae (Coleman, 2007). We compared the predicted ITS2 secondary structure of the novel Black Sea strains, IBSS-Cr-7S4, IBSS-Cr-4.2G and IBSS-Cr-4.19, and their closest relatives that are available in GenBank to assess their genetic distinction and taxonomic status (Figs 46 and 47).

The predicted ITS2 secondary structures for all three strains folded into typical eukaryotic four-helix conformations, with helix III being the longest (Coleman, 2007) (Fig. 46). A characteristic unpaired U–U mismatch in helix II was observed only in IBSS-Cr-7S4, whereas IBSS-Cr-4.19 exhibited unpaired pyrimidines C–C, and IBSS-Cr-4.2G showed an unpaired A–C mismatch.

The ITS2 secondary structures of strains IBSS-Cr-4.19 and IBSS-Cr-4.2G were highly congruent in terms of relative helix lengths, inter-helical spacing and the localization of internal loops and bulges, differing by only four CBCs. Conversely, the ITS2 secondary structure of strain IBSS-Cr-7S4 exhibited significant divergence, with 28 and 21 CBCs compared to IBSS-Cr-4.19 and IBSS-Cr-4.2G, respectively, clearly supporting its status as a distinct species.

Phylogenetic analyses (Fig. 42, Supplementary figs S2–S4) indicated that the strains IBSS-Cr-4.19 and IBSS-Cr-4.2G are closely related to four Brazilian strains, of which only strain MN UFRJ-BrCr9 has ITS2 sequence available. It differs from IBSS-Cr-4.19 by a single CBC and three semi-CBCs (all in helix I), and from IBSS-Cr-4.2G by three semi-CBCs (two in helix I and one in helix IV) (Fig. 47). This minor divergence indicates that MN UFRJ-BrCr9 and IBSS-Cr-4.2G are conspecific, and IBSS-Cr-4.19 represents a closely related lineage.

CBCs within ITS2 are widely employed as a reliable molecular criterion for species delineation in eukaryotes (Coleman, 2007). However, recent studies have identified cases of CBCs occurring within a single species in certain algal groups, such as the Chlorophyceae, orders Ulvales and Volvocales (Caisová *et al.*, 2011, 2013; Temraleeva & Bukin, 2022). These authors regarded such CBCs as intraspecific polymorphisms rather than as markers of speciation, thereby challenging the 'one-CBC-criterion' as a universal rule for species separation,

and suggesting an integrative approach to species delineation. Following this framework, the CBCs identified between IBSS-Cr-4.19, IBSS-Cr-4.2G and the Brazilian strain MN UFRJ-BrCr9 are interpreted here as intraspecific genetic variability, given their identical molecular signatures in other markers and congruent phylogenetic positioning.

Congruence between molecular and morphological signals

To evaluate the congruence between the morphological variability and phylogenetic relationships within the Pyrenomonadaceae, key diagnostic traits were mapped onto the combined phylogenetic tree (Fig. 42). The taxon sampling strategy targeted strains for which molecular data were supplemented by robust morphological descriptions or original type designations, whenever available.

The generic differentiation within the Pyrenomonadaceae has historically been based on conventionally accepted LM and SEM-defined morphological traits (Hill & Wetherbee, 1989; Kugrens *et al.*, 1999; Majaneva *et al.*, 2014). Traditional classification attributed taxonomic significance to the presence of rectangular (*Rhodomonas*) or hexagonal (*Rhinomonas*) plates versus a continuous sheet-like inner periplast component (*Storeatula*). Additionally, genera are delineated by the presence (*Rhodomonas* and *Rhinomonas*) or absence (*Storeatula*) of a true furrow, and the presence (*Rhodomonas*) or absence (*Rhinomonas*) of a mid-ventral band (Hill & Wetherbee, 1988, 1989; Hill, 1991). The discussion on the admissibility and validity of dividing the Pyrenomonadaceae into these three genera was opened since Hill & Wetherbee (1989) emended the *Pyrenomonas* genus invented by Santore (1986), proving that it was synonymous to *Rhodomonas* (Karsten, 1898) with *Rhodomonas baltica* as the generitype.

Since then molecular data have been applied to the cryptophytes taxonomy, and it has become increasingly evident that the morphological traits traditionally employed for taxonomic classification within the Pyrenomonadaceae frequently fail to correspond to the underlying genetic diversity (Deane *et al.*, 2002; Hoef-Emden *et al.*, 2002; Majaneva *et al.*, 2014; Daugbjerg & Devantier, 2024; Khanaychenko *et al.*, 2022; this study).

Analysis of the morphological traits distribution across the tree revealed that neither IPC type nor gullet-furrow structure, either individually or in combination, provide sufficient support for the recovered branching order to unambiguously delineate major clades (Fig. 42). While a mid-ventral band appears to be a relatively consistent diagnostic feature of Clade A, its reported presence in *Rhodomonas maculata* (Hill & Wetherbee, 1989) from Clade C challenges the taxonomic usefulness of this structural character as a reliable clade-specific marker.

The incompatibility of IPC type with the topology of molecular trees has been revealed in many cryptomonad groups (Deane *et al.*, 2002; Hoef-Emden & Melkonian, 2003; Hoef-Emden, 2007, 2012; Majaneva *et al.*, 2014; Altenburger *et al.*, 2020; Khanaychenko *et al.*, 2022; Daugbjerg & Devantier, 2024), thereby the monophyly of the genera with periplast-based delineation and their taxonomy have been questioned (Hoef-Emden & Melkonian, 2003; Lane *et al.*, 2005; Shalchian-Tabrizi *et al.*, 2008; Majaneva *et al.*, 2014). In the present study, the discrepancy between morphological and molecular datasets is clearly demonstrated by three closely related Black Sea cryptophyte strains. Strains IBSS-Cr-4.2G and IBSS-Cr-4.19 exhibited significant morphological disparities, differing in both their gullet-furrow complex and periplast structure (Figs 14–25 vs. 26–37), yet are nearly identical in rRNA and ITS2 structures (Figs 42 and 46). Conversely, the morphologically similar strains IBSS-Cr-7S4 and IBSS-Cr-4.2G (Figs 1–13 and 14–25) were found to be distantly related based on molecular data (Figs 42 and 46).

These findings reinforce the consensus that traditional taxonomic markers in the Pyrenomonadaceae, such as IPC type, gullet-furrow structure, and presence/absence of mid-ventral band, are often unreliable for defining natural species and generic boundaries. This pervasive incongruence necessitates a shift towards an integrative approach, where stable molecular signatures and life-history data take priority over plastic morphological characters.

Evidence of dimorphism

In order to discern the long-suspected dimorphism within the Pyrenomonadaceae, the potential morphological intra-strain variability was first examined in three strains with a sheet-like inner periplast component, including *Rhodomonas storeatuloformis* (IBSS-59) and novel isolates, IBSS-Cr-7S4 and IBSS-Cr-4.19. Cells were sampled from clonal cultures at the exponential, stationary and ageing growth stages to capture any potential life-cycle transitions. A thorough examination of the cell external morphology was conducted using SEM (at least 100 cells per strain) to discern intra-strain variations in the inner periplast component structure. Extensive SEM screening focused specifically on size extremes, as haploid-diploid transitions in cryptophytes typically involve significant size differentiation and a shift from a sheet-like to a plate-like IPC (Hill & Wetherbee, 1986; Hill, 1991; Hoef-Emden & Melkonian, 2003; Altenburger *et al.*, 2020; van den Hoff *et al.*, 2020).

SEM observations revealed no intra-strain variation in IPC structure; all cells, regardless of size or growth phase, invariably possessed a continuous sheet-like periplast (e.g. Fig. 8). No spontaneous transition between morphotypes was observed in routinely maintained cultures, suggesting that the strains remained in a stable ploidy state under the provided conditions.

While cell morphology remained invariable within each individual culture, flow cytometry confirmed a difference in DNA content between genetically near-identical strains possessing distinct morphotypes: IBSS-Cr-4.19 (continuous, sheet-like IPC) and IBSS-Cr-4.2G (plated IPC). Quantitative cytofluorometry revealed two distinct, non-overlapping peaks of green fluorescence, corresponding to the relative cellular DNA content (Fig. 48). The fluorescence intensity of strain IBSS-Cr-4.19 was approximately twice that of strain IBSS-Cr-4.2G (median = 22,198 vs. 11,250, respectively). Furthermore, the fluorescence intensity in another strain with sheet-like IPC (IBSS-Cr-7S4) was comparable to that of IBSS-Cr-4.19 (not shown). These findings demonstrate that the morphological divergence between strains IBSS-Cr-4.19 and IBSS-Cr-4.2G represents different stages of a single haplo-diploid life cycle rather than distinct taxa. The haplomorph is distinguished by plated IPC and a gullet-furrow complex, while the diplomorph is characterized by a continuous sheet-like IPC and the absence of a furrow.

A further study employed molecular phylogenetic data to infer evidence of hidden dimorphism across the Pyrenomonadaceae. Our analysis included all available molecular data related to *Storeatula* strains to identify phylogenetically close yet morphologically distinct strains that likely represent alternative morphs within a single life cycle. The taxon sampling comprised 15 strains of *Storeatula* spp. and strains with *Storeatula*-like morphology, including *Rhodomonas storeatuloformis* and two newly isolated strains, IBSS-Cr-7S4 and IBSS-Cr-4.19. Available morphological examinations of each of the strains under consideration confirmed a simple gullet structure lacking a furrow and a continuous, sheet-like inner periplast component.

In the phylogenetic tree (Fig. 42), the *Storeatula*-like strains nested among the *Rhodomonas* and *Rhinomonas* strains rather than formed a single monophyletic clade, suggesting hidden dimorphism in at least some of the taxa within the Pyrenomonadaceae. Within Clade B, the *Storeatula major* strain SZN-T2 was genetically identical to strains identified as *Rhodomonas baltica* (NIES700 and CCMP747), *Rhodomonas irregularis* (NIES698) and an unidentified *Rhodomonas* sp. (BEA 0120B). The strain SZN-T2 was isolated from the Gulf of Naples in the Mediterranean Sea, Italy and was assigned to *Storeatula major* based on its large size, V-shaped vestibulum lacking a furrow and sheet-like IPC (Cerino & Zingone, 2006: fig. 40). Of the genetically identical *Rhodomonas* strains in this subclade, only the morphology of *Rhodomonas irregularis* NIES698 has been examined. This strain (originated from the type strain Pl60 BC, CCAP 979/7 *Cryptomonas irregularis*) was isolated in Plymouth, Devon, UK by Butcher in 1960. Its morphology was described by Butcher (1967) based on LM observations (well-marked furrow closing rapidly into a short gullet) and was later supplemented by TEM examination of the internal cell structure, from which the inner periplast plates were clearly identifiable (Erata & Chihara, 1989: fig. 5).

In Clade C, *Storeatula* sp. 1 (strain SZN-C1) and *Rhinomonas reticulata* (strain SZN-C48b) were closely allied to each other, differing by a single nucleotide substitution (deletion) in an overlapping 1524-bp nuclear SSU rDNA fragment. Both strains were isolated from the Gulf of Naples, Mediterranean Sea, Italy. *Storeatula* sp. 1 possessed a gullet lacking a furrow and a continuous, sheet-like IPC (Cerino & Zingone, 2006: fig. 42). In contrast, *Rhinomonas reticulata* was characterized by IPC with discrete hexagonal plates (Cerino & Zingone, 2006: figs 26, 27). Furthermore, *Storeatula* sp. 1 SZN-C1 was genetically identical to *Rhodomonas* sp. strain CCMP740, however, the latter has no associated morphological data to allow comparison.

Despite being collected from geographically isolated populations in the Gulfs of Trieste and Naples, *Storeatula* sp. 2 T1 was genetically identical to *Rhodomonas* sp. 3 SZN-C42 (Clade A). The strains also differed in morphology, with sheet-like IPC and a gullet lacking a furrow in *Storeatula* sp. 2 (Cerino & Zingone, 2006: fig. 44) versus a prominent furrow extending for more than a third of the cell length and discrete rectangular plates in IPC in *Rhodomonas* sp. 3 (Cerino & Zingone, 2006: fig. 38).

Most notably, the high genetic similarity (p-distance 0.095) and identical molecular signatures between the morphologically divergent Black Sea strains IBSS-Cr-4.19 and IBSS-Cr-4.2G (Figs 14–25 vs. 26–37), combined with their confirmed difference in ploidy (Fig. 48), conclusively demonstrate that these strains represent alternative life-cycle stages of a single species.

Storeatula major strain CCMP320 was nested in a well-supported subclade together with the *Rhinomonas pauca* and unidentified *Rhinomonas* and *Rhodomonas* strains. However, the lack of morphological observations related to this *Storeatula* strain prevents matching. Similarly, the close phylogenetic relation of *Storeatula*-like strains IBSS-Cr -7S4 to the *Rhodomonas* strains with unknown morphology (2–3 nucleotide substitutions in nuclear SSU rDNA fragments of 1707–1729 bp) makes it impossible to identify different morphs within these taxa.

Taxonomic implications and further perspectives

Despite phylogenomic studies consistently validating the Pyrenomonadaceae as a robust natural lineage, its classification is hindered by significant taxonomic incongruity, as traditional morphological boundaries fail to align with emerging molecular evidence. Consequently, the resulting systematic instability necessitates a comprehensive taxonomic revision. Historically, the structural differences of the inner periplast component have been used to justify the separation of genera, particularly for the genus *Storeatula* (Hill, 1991). However, phylogenetic studies of the family (e.g. Deane *et al.*, 2002; Majaneva *et al.*, 2014; Khanaychenko *et al.*, 2022; Daugbjerg & Devantier, 2024; this study) revealed that strains assigned to *Storeatula* based on their morphology were distributed across the *Rhodomonas* and *Rhinomonas* rather than forming a separate clade (Fig. 42). The lack of genetic data of the authentic strain for the generitype, *Storeatula major*, further complicates the taxonomic state of this genus. Although the *Storeatula*-like morphotypes have been previously hypothesized to represent an alternative stage in the life cycle of *Rhodomonas* and *Rhinomonas* (Hoef-Emden & Melkonian, 2003; Majaneva *et al.*, 2014; Solarska *et al.*, 2023; Daugbjerg & Devantier, 2024), the dimorphism has not been recovered for any Pyrenomonadaceae species to date.

Our data suggest that *Storeatula*-like morphotypes with sheet-like IPCs represent diploid stages of a single dimorphic life cycle rather than distinct evolutionary lineages (Figs 42, 48). Through broad taxon sampling, we identified strains across the Pyrenomonadaceae that are structurally dissimilar regarding vestibular invagination and the inner periplast structure, yet genetically identical (Fig. 42). Based on an integrative approach combining molecular phylogenetic data, morphological observations and DNA content measurements, we suggest abolishing the genus *Storeatula*, relegating its nomenclatural status to an alternative life-cycle stage within other Pyrenomonadaceae.

We propose that further descriptions of Pyrenomonadaceae taxa require consideration of potential dimorphism, as morphological diagnoses based on the periplast or gullet-furrow complex are unreliable for species delineation in the absence of cytological data. Without determining the ploidy level, there is a risk of misidentifying a life-cycle stage as a novel taxonomic unit, further complicating the already unstable nomenclature of the group.

While our findings suggest a way towards merging several genera, a complete taxonomic revision of the Pyrenomonadaceae remains currently unattainable due to nomenclatural instability. The primary limitation is the current taxonomic and nomenclatural challenges surrounding the genus *Rhodomonas*, particularly generitype *Rhodomonas baltica*. The type specimens of *Rhodomonas baltica* have been examined by Karsten by light microscopy more than a century ago (Karsten, 1898). The original description of *R. baltica* is deficient in terms of detail and clarity (e.g. the central pyrenoid was likely misidentified as the nucleus) and lacks the ultrastructural detail (such as periplast type or gullet-furrow structure). Subsequent findings and descriptions attributed to *R. baltica* are dubious regarding their identity with the type material, as a wide range of cryptomonads have similar shapes and red chloroplasts (as Butcher (1967) noted 'of all the forms described as *Rhodomonas baltica*, only the original one collected may bear this name').

Previous attempts to stabilize the genus, such as the emended diagnosis by Hill and Wetherbee (1989), relied on unsequenced strains isolated from Europe to Australia, further widening the gap between morphological and molecular data. The co-identity of these strains to *Rhodomonas baltica* was inferred based on the similarity of the LM-observed cells to the original Karsten drawings. While a substantial advancement in the understanding of *R. baltica* was achieved through the application of electron microscopy, which led to an update in the available morphological details and resulted in Hill and Wetherbee amending the diagnosis of the genus (Hill & Wetherbee, 1989), the applicability of these structural details to phylogenetic studies remains uncertain. Conversely, the morphology of strains labelled as *R. baltica* in the GenBank collection remains unstudied or is restricted to the uninformative LM micrographs available in the culture collection metadata.

Despite evident morphological distinctions in the gullet-furrow complex and periplast structure, molecular analyses consistently revealed paraphyly within the *Rhodomonas*/*Rhinomonas*/*Storeatula* group (Deane *et al.*, 2002; Hoef-Emden *et al.*, 2002; Shalchian-Tabrizi *et al.*, 2008; Majaneva *et al.*, 2014; Daugbjerg & Devantier, 2024; this study). Novarino (1991) raised concerns regarding the stability of the morphological characteristics used to differentiate between the genera *Rhodomonas* and *Rhinomonas*, noting that the furrow may be an artefact resulting from SEM preparation (Novarino, 1991). Furthermore, the interpretation of the periplast plates shape may be affected by hypotonic conditions (Gantt, 1971) or centrifugation (Kugrens & Lee, 1987). Specifically, Santore (1977) highlighted that while the underlying periplast architecture is a stable pattern defined by plate shape and trichocyst distribution, the superficial appearance is easily distorted in whole-mounted SEM cells. A slight offset of adjacent plate rows relative to the constant position of the trichocysts can create a honeycomb-like pattern of regular

hexagons, even if the plates are rectangular themselves (Santore, 1977: fig. 23). This misidentification is reinforced during the drying and mounting procedures, which can physically compress or displace these delicate layers. While SEM observations of whole-mounted cells effectively distinguish between the sheet-like or plated appearance of the IPC, the freeze-fracture and freeze-etch techniques provide more detailed insight into the ultimate architecture of the cell surface, including the precise identification of plate shape (e.g. Kugrens & Lee, 1987; Wetherbee *et al.*, 1987). Despite being recommended for taxonomic studies (Novarino, 2012), these techniques are scarcely employed in surveys of the Pyrenomonadaceae taxa. To date, the precise shape of IPC plates has been evaluated using the freeze-fracture /etch technique in only a limited number of taxa, such as *Rhodomonas baltica, R. salina, R. maculata* (Hill & Wetherbee, 1989), *R. chrysoidea* (Kugrens & Lee, 1987), *R. stigmatica* (Hill, 1991), *Pyrenomonas ovalis* (Kugrens *et al.*, 1999) and *Rhinomonas pauca* (Hill & Wetherbee, 1988). Consequently, to accurately assess the diagnostic value of plate morphology in Pyrenomonadaceae taxonomy, further high-resolution structural data across a broader range of taxa is required to distinguish true biological variation from preparation-induced artefacts.

Recent studies of the Pyrenomonadaceae have revealed the obvious non-independence of some *Rhodomonas* and *Rhinomonas* species with nearly identical SSU rDNA sequences identified during molecular genetic analysis (Majaneva *et al.*, 2014; Daugbjerg & Devantier, 2024; this study), posing a doubt for species delineation within the genera. These issues, combined with the lack of comprehensive characterization for many Pyrenomonadaceae species (e.g. see Supplementary table S1), complicate a robust revision of the genus *Rhodomonas* and the broader family. The lack of type material and the uncertainty surrounding the phylogenetic position of the *Rhodomonas* type species prevent a revision of the entire Pyrenomonadaceae within the scope of this study. Nevertheless, our results contribute to further delineation of the taxa within the family, implying that *Rhodomonas* and *Rhinomonas* (Clade B + C) may be congeneric. In addition to the recognition of the hidden dimorphism in the Pyrenomonadaceae, which warrants the suppression of the genus *Storeatula*, a set of unique molecular signatures identified in this study provides a basis for distinguishing natural groups within the family.

The establishment of *Eomonas* gen. nov. provides a formal taxonomic circumscription for a distinctly divergent lineage (Clade A), clearly distinguished by unique molecular signatures. This newly defined genus accommodates both previously recognized taxa and two newly described species, *Eomonas fusiformis* sp. nov. and *Eomonas vitalis* sp. nov., further highlighting the previously unrecognized diversity within this lineage. In the subsequent section, we present a molecular differential diagnosis for the genus *Eomonas*, distinguishing it from the herein redefined *Rhodomonas* complex.

In order to restore nomenclatural stability, the *Rhodomonas* complex is designated herein as a monophyletic yet polymorphic assemblage formerly encompassing *Storeatula, Rhinomonas* and *Pyrenomonas* taxa. This taxonomic status remains pending further formal revision, until the nomenclatural uncertainties surrounding the generitype, *Rhodomonas baltica*, are fully resolved and the gap between historical morphological and modern molecular data is sufficiently bridged. In this group, a revision of the *Rhodomonas salina* complex is performed to clarify the boundaries of this widely recognized but taxonomically confused lineage based on molecular phylogeny and morphologically validated strains. Finally, designation of several ambiguous historical taxa as *nomina confusa* facilitates a more streamlined, molecular-based taxonomy that reduces the risk of misidentification.

Taxonomic summary

The genus Storeatula

We propose the abolition of the genus *Storeatula* and the formal synonymization of its described strains with other taxa within the Pyrenomonadaceae. This taxonomic reassessment is based on the dimorphic life cycle identified in the present study, which reveals that *Storeatula*-like morphotypes represent the diploid stage of various lineages within the family.

Establishment of Eomonas *gen. nov.*

Clade A serves as the basis for the establishment of a new genus, justified by its clear phylogenetic distinctness, high statistical support and unique molecular signatures. *Eomonas marina* (syn. *Rhodomonas marina*) is designated as the type species, as it represents the earliest described taxon (Dangeard, 1892) and has recently undergone a comprehensive morphological and molecular revision (Daugbjerg & Devantier, 2024). The new genus further encompasses two previously taxonomically recognized taxa, *Eomonas abbreviata* and *Eomonas duplex*, now proposed as new combinations. Species descriptions were emended to incorporate the molecular signatures identified in the present study.

The newly described strain IBSS-7S4 is recognized as the diploid stage in the life cycle of a distinct new dimorphic species, *Eomonas fusiformis*. Its corresponding alternative morphotype is represented by

the strain *Rhodomonas* sp. 3, previously isolated from the Mediterranean Sea (Cerino & Zingone, 2006). All strains comprising this highly supported clade (1.0/100) are considered conspecific based on a low p-distance (0–0.7%). Morphological description of *Rhodomonas* sp. 3 reported by Cerino and Zingone (2006) is attributed to the haploid life-cycle stage of a new dimorphic species.

The lineage comprising *Storeatula* CCMP1868 strain and its subclones remains formally undescribed *Eomonas* sp. due to the lack of morphological data and is tentatively considered as an undescribed diplomorph with undiscovered yet haplomorphic stage.

Strains IBSS-4.2G and IBSS-4.19, along with closely related Brazilian strains, are considered conspecific based on fully supported tree topology and negligible genetic divergence of the comprised strains (p-distance of 0–0.1%). We interpret a number of CBCs identified between the Black Sea IBSS-Cr-4.19, IBSS-Cr-4.2G and the Brazilian strain MN UFRJ-BrCr9, as intraspecific genetic variability, given their identical molecular signatures in other markers, congruent phylogenetic positioning and the confirmed haploid-diploid relationship between the Black Sea isolates. Consequently, a novel dimorphic species, *Eomonas vitalis*, is described, with IBSS-4.2G designated as the haplomorph and IBSS-4.19 as the diplomorph stage within the same life cycle.

Eomonas Saburova, Khanaychenko, Nikolaeva & Aleoshin gen. nov.

DIAGNOSIS: Motile, marine cryptophytes characterized by a dimorphic life cycle, with two morphologically distinct haploid and diploid stages. Cells of both stages with subapical vestibulum and two unequal flagella, with either a single, deeply bilobed, H-shaped, parietal chloroplast with lobes connected by a small dorsal conjunction and a single central pyrenoid or, less commonly, with lobes completely separated into two chloroplasts with two pyrenoids, red to brownish in colour, containing phycoerythrin Cr-PE-545. Nucleomorph is embedded into the pyrenoid. Haplomorph with a straight longitudinal furrow of varying length extending into a tubular gullet, with a conspicuous mid-ventral band; inner periplast component composed of small discrete polygonal plates arranged in longitudinal spiral rows. Diplomorph with V-shaped vestibulum lacking furrow and continuous sheet-like periplast with randomly spaced pores to accommodate ejectosomes.

TYPE SPECIES: *Eomonas marina* (P.A.Dangeard) Saburova, Khanaychenko, Nikolaeva & Aleoshin comb. nov.

ETYMOLOGY: The prefix 'eo-' is derived from the Greek ἑως (Eos), the ancient Greek term for dawn or early morning light and the name of the Greek goddess of the dawn often named as 'rosy-fingered', referring to the genus arising from within the *Rhodomonas* lineage along with the natural reddish colouration of the organisms comprising the genus.

MOLECULAR SIGNATURES: Hairpin 10 of nuclear 18S rRNA is shortened or has motif 5′-AGGTCCGAC**G**CA**A**GGAGGACTG-3′ (synapomorphic characters are bolded and underlined) (Fig. 43); Nucleomorph 18S rRNA has motif 5′-GCTCGTAGTCGAAT-**C**-3′ and 5′-GCGTGAGTCAT-**C**-AACTCGCGCT-3′ (symplesiomorphic characters are bolded and underlined; only valid within the Pyrenomonadaceae).

DIFFERENTIAL DIAGNOSIS: Synapomorphy in nucleomorph 18S rRNA, motif 5′-**C**-TRGCGGCRGCG-3′ (synapomorphic character is bolded and underlined); Symplesiomorphies in the nuclear 5.8S rRNA, motif 5′-RTG **G**KBG**AC**CATRAGYACGTCTGTY**T**GA<+53 bp upstream>-3′ (Fig. 45). Symplesiomorphies in hairpin 11 of nuclear 18S rRNA, motif 5′-CC**T**T**TAY**GGT-3′ (Fig. 44) (symplesiomorphic characters are bolded and underlined; only valid within the Pyrenomonadaceae).

SPECIES INCLUDED: *Eomonas marina* (P.A. Dangeard) comb. nov.; *Eomonas abbreviata* (Butcher *ex* D.R.A.Hill & R.Wetherbee) comb. nov.; *Eomonas duplex* (D.R.A.Hill & R.Wetherbee) comb. nov.; *Eomonas fusiformis* sp. nov.; *Eomonas vitalis* sp. nov.

Eomonas abbreviata (Butcher *ex* D.R.A.Hill & R.Wetherbee 1989) Saburova, Khanaychenko, Nikolaeva & Aleoshin comb. nov.

BASIONYM: *Rhodomonas abbreviata* Butcher *ex* D.R.A.Hill & R.Wetherbee 1989: Phycologia 28: 154.

SYNONYM: *Cryptomonas abbreviata* Butcher 1967: 46 (*nom. inval.*, typ. non desig.); *Pyrenomonas abbreviata* (Butcher) Santore 1986: 80 (*nom. inval.*)

EMENDED DIAGNOSIS: Cells irregularly obovate with unequally convex sides; anterior end subacute or rounded and somewhat obliquely truncate, posterior end usually acute or elongate in dorsal view; narrowly cylindrical with acute or rounded ends in lateral view; strongly dorso-ventrally compressed; 10–14 μm long, 6–7 μm wide and 5–6 μm deep. Two flagella of unequal length emerge from a subapical vestibulum. Chloroplast single, parietal, extending approximately 1/2 of the cell length, markedly lobed at edges, olive yellow to gold in colour. Pyrenoid single, encircled by an irregular sheath of starch grains. Nucleomorph embedded in a chloroplast-envelope invagination into the pyrenoid. Gullet-furrow complex extends 1/2 of cell length, lined

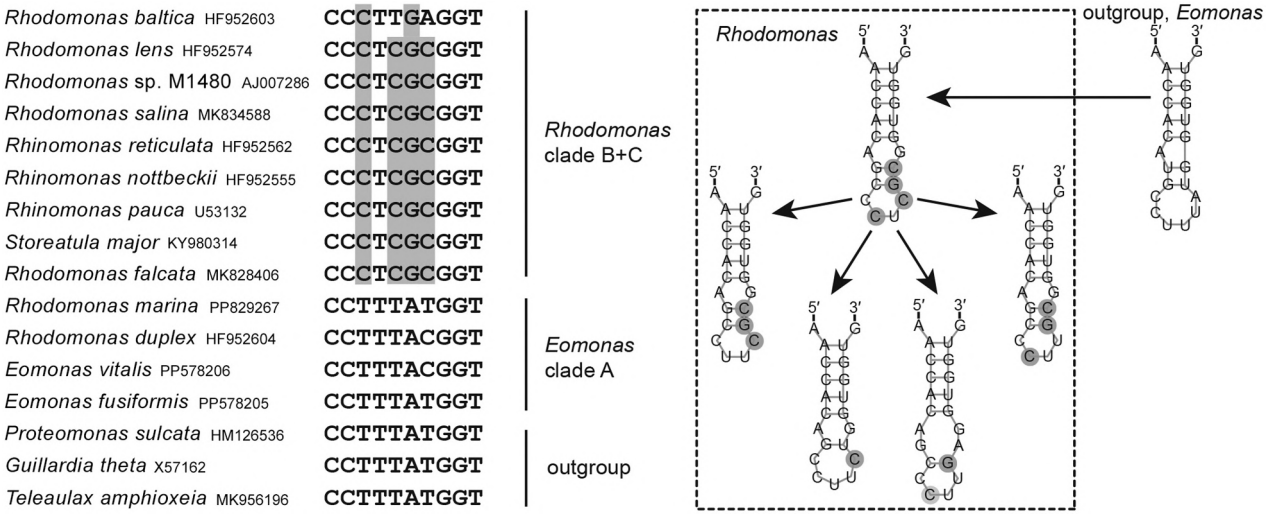


Fig. 44. Molecular signature of the genus *Rhodomonas*. Left: alignment of hairpin 11 of SSU rRNA. Right: predicted secondary structures of hairpin 11 of SSU rRNA for the genus *Eomonas*, which retains the plesiomorphic structure, and five structural variants for the genus *Rhodomonas*. Synapomorphic nucleotides for the genus *Rhodomonas* are highlighted in grey.

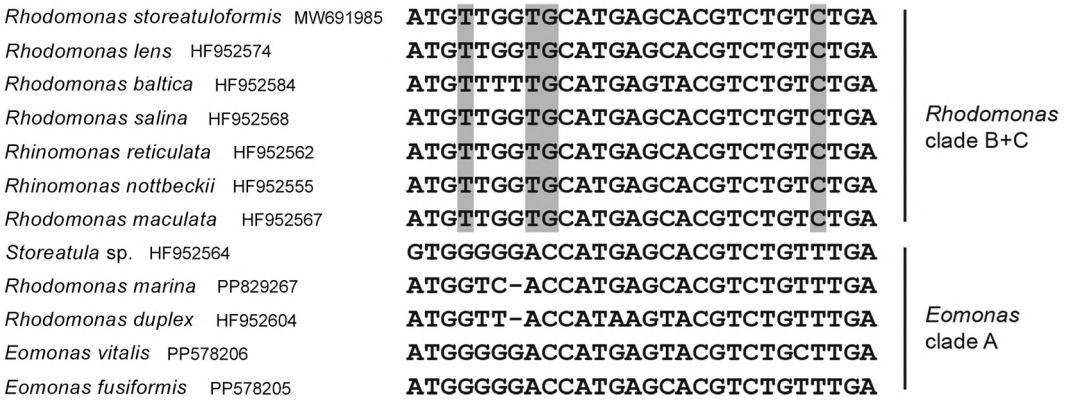


Fig. 45. Molecular diagnosis of *Eomonas* gen. nov. Alignment of 5.8S rRNA motif showing plesiomorphy in *Eomonas* strains and apomorphy in *Rhodomonas* strains. Synapomorphic nucleotides for the genus *Rhodomonas* are highlighted in grey.

with numerous large ejectosomes; furrow long and vertical. Nucleus in the posterior end; contractile vacuole in the anterior end.

LECTOTYPE: (designated by Hill & Wetherbee, 1989): Butcher 1967: pl. VI, fig. 3.

TYPE LOCALITY: Rock pool at Jerbourg, Guernsey, UK.

AUTHENTIC STRAIN: CCAP 976/16 (isolated from Guernsey, Channel Islands by Butcher in 1960 (orig. design. SJ1.BC 28/2), reacquired from Cologne Culture Collection).

GENE SEQUENCE DATA: CCAP 976/10, nuclear18S rRNA (U53128); CCAP 976/10 nucleomorph 18S rRNA (U53I27). Note: an inaccuracy was identified in the GenBank metadata, where strain CCAP 976/16 was erroneously recorded as 976/10, although the correct strain number, 976/16, was specified in the original publication (Cavalier-Smith *et al.*, 1996: table 1).

MOLECULAR SIGNATURE: Autapomorphy in the nuclear 18S rRNA: 5′-ACCATG**T**CATTTA<84 bp upstream>-3′ (autapomorphic site is bolded and underlined).

***Eomonas duplex* (D.R.A.Hill & R.Wetherbee) Saburova, Khanaychenko, Nikolaeva & Aleoshin comb. nov.**

BASIONYM: *Rhodomonas duplex* D.R.A.Hill & R.Wetherbee 1989: Phycologia 28: 153, figs 32–37.

SYNONYM: *Cryptomonas appendiculata* Butcher 1967: 46–47 (*nom. illeg.*, non *Cryptomonas appendiculata* Schiller 1957: 26).

EMENDED DIAGNOSIS: Cells narrowly obovate to somewhat clavate, with an undulate margin, rounded anterior and acute posterior in ventral view; ovate to obovate, often with undulate sides, with truncate, more or less rostrate anterior end and acute, produced or at times obtuse posterior end in lateral view; laterally compressed; 13–15 μm long, 5–6 μm

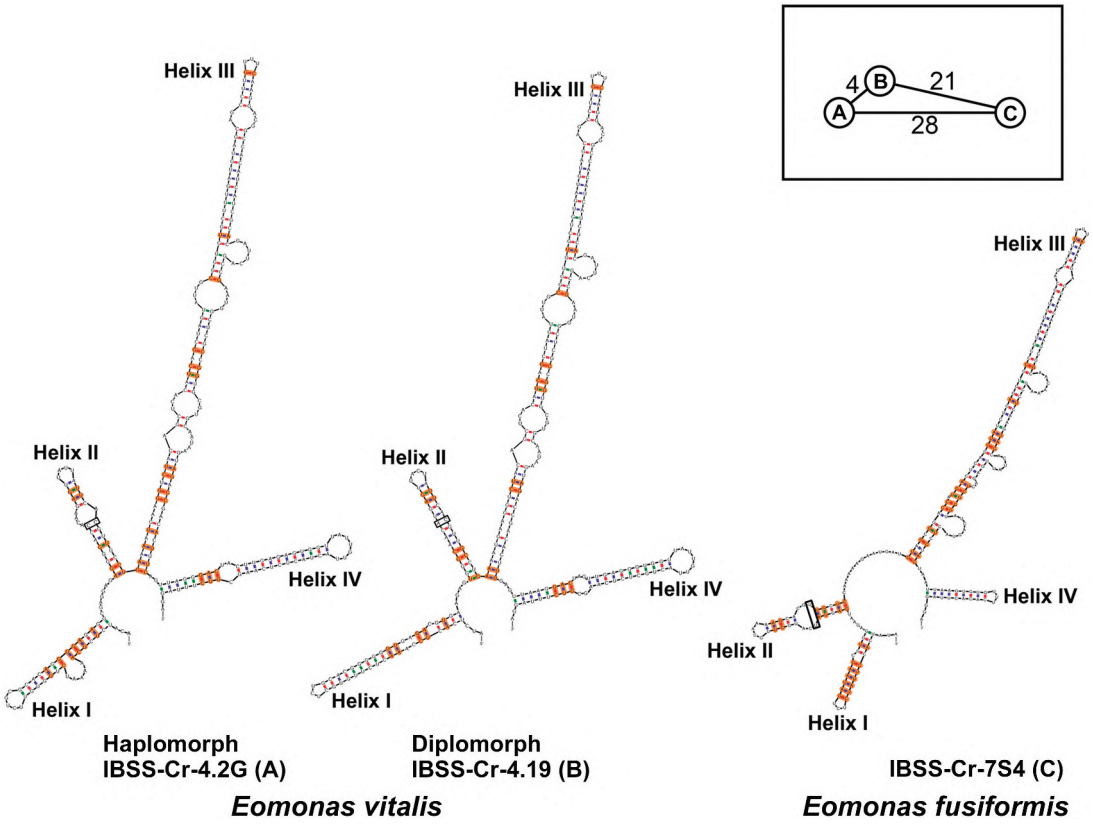


Fig. 46. Predicted secondary structures of ITS2 for *Eomonas vitalis* sp. nov. (strains IBSS-Cr-4.19 and IBSS-Cr-4.2G), and *Eomonas fusiformis* sp. nov. (strain IBSS-Cr-7S4). Helices are numbered according to Coleman (2000). Typical unpaired mismatches in helices II are marked by rectangles. CBCs are marked in orange. Pairwise quantities of CBCs between strains are shown in the frame.

wide, 4.5–5.5 μm deep. Two flagella unequal in length emerge from subapical vestibulum. Two chloroplasts for the majority of the life cycle, daughter cells initially contain a single chloroplast, with replication occurring in the immediate aftermath of cell division. Chloroplasts parietal, extending approximately 3/4 of the cell length, lobed, bright red to orange-yellow in colour, containing Cr-PE 545. Two conspicuous pyrenoids, each encircled by an irregular starch sheath. Nucleomorph in each pyrenoid, embedded in a chloroplast-envelope invagination into pyrenoid. Gullet-furrow complex short, lined with 3–4 rows of plain ejectosomes; furrow conspicuous, 1/5 of the cell length. Inner periplast component consists of longitudinal rows of small, more or less rectangular plates. Surface component delicate but complete layer of intertwining fibrils. Mid-ventral band present. Nucleus in posterior end.

HOLOTYPE: Hill & Wetherbee, 1989: fig. 35, based on strain MUCC Cr #54 originated from Mary Parke's isolate Plymouth 23.

TYPE LOCALITY: Port Erin, Isle of Man, UK.

AUTHENTIC STRAINS. Plymouth 23; MUCC Cr #54; CCAP 979/13.

GENE SEQUENCE DATA: strain NIES765, nuclear 18S rRNA (AB240960), nuclear 18S rRNA, ITS/5.8S rRNA, 28S rRNA (HF952604), nucleomorph 18S rRNA (HF952620) [non-authentic strain isolated in Yaga Okinawa, Japan].

MOLECULAR SIGNATURE: Autapomorphy in the nuclear 18S rRNA: 5′-<+797 bp upstream>TGGGACC GGAGTAATGA-3′ (autapomorphic site is bolded and underlined).

Eomonas fusiformis Saburova, Khanaychenko, Nikolaeva, Rylkova & Aleoshin sp. nov. (Fig. 1–13).

DIAGNOSIS: Dimorphic with stable, dissimilar haploid and diploid morphs within strains. In both stages, cells elongated, ellipsoidal to fusiform in dorsal/ventral view, with round to narrowed anterior and narrowed to pointed posterior, with somewhat rhinose apex in lateral view. Two unequal flagella emerge from subapical vestibulum. Chloroplast single, parietal, deeply bilobed, light-brown in colour, contains Cr-PE 545. Central pyrenoid of irregular, bevelled shape, located dorsally, encircled by starch grains. Gullet lined with ejectosomes. Nucleus located posteriorly.

DIPLOMORPH cells 17.5–27.4 μm long, 8.0–12.5 μm wide. Vestibulum V-shaped, with a fold depressed on the left side, furrow absent. Inner

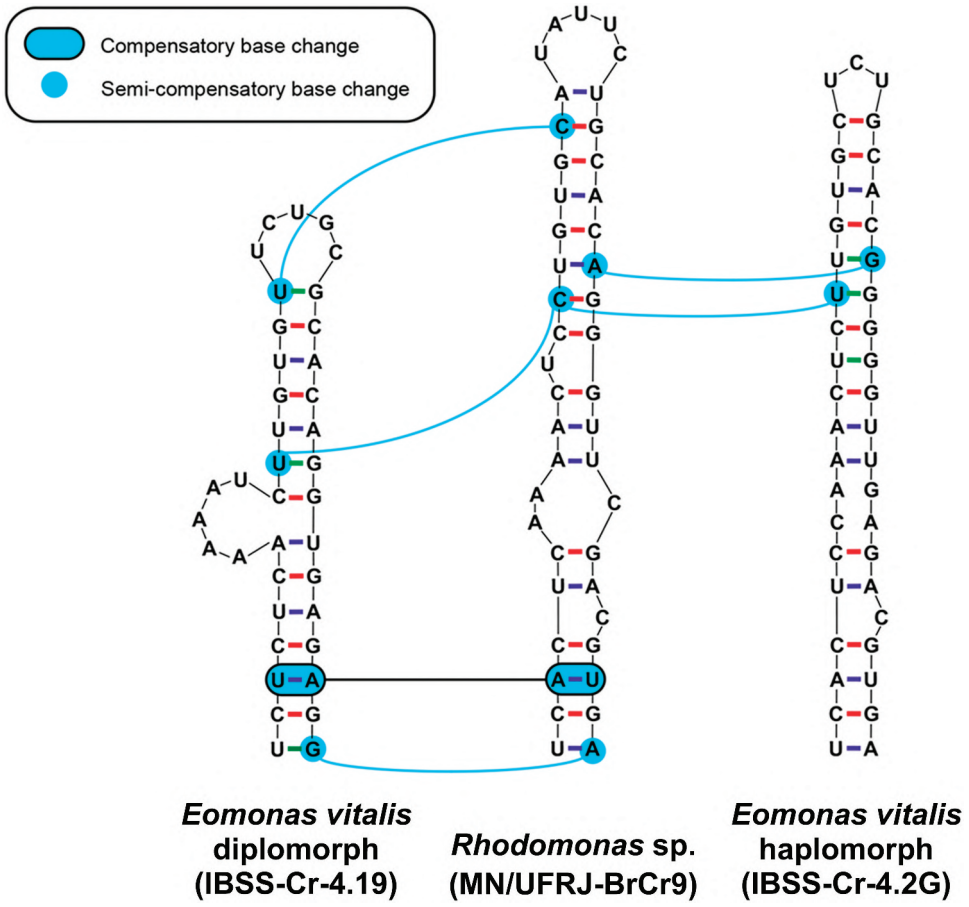


Fig. 47. Predicted secondary structures of ITS2 helix I for *Eomonas vitalis* sp. nov. (strains IBSS-Cr-4.19 and IBSS-Cr-4.2G) and closely related *Rhodomonas* sp. MN/UFRJ-BrCr9. Helices are numbered according to Coleman (2000).

periplast component continuous sheet-like, with numerous small ejectosomes underneath.

HAPLOMORPH cells 14.0–23.0 μm long, and 6.0–8.5 μm wide. Gullet-furrow complex 1/3 of the cell length, furrow long. Inner periplast component consists of small rectangular plates in a spiral configuration. Mid-ventral band present.

HOLOTYPE: SEM stub with material of the strain IBSS-Cr-7S4 (stable diplomorph strain), fixed and critical-point dried, deposited at the Algal Herbarium (LE) of the Komarov Botanical Institute, St. Petersburg, Russia (ref. number A0004143). The glutaraldehyde and alcohol-fixed samples of the strains are also kept at the Department of Aquaculture and Marine Pharmacology of IBSS under accession number A256-1-Cr-7S4 and A256-2-Cr-7S4, respectively.

PARATYPE: Illustrations of *Rhodomonas* sp. 3 SZN-42 (haplomorph) in Cerino & Zingone (2006: figs 37, 38) and *Storeatula* sp. 2 SZN-C14 (diplomorph) in Cerino and Zingone (2006: figs 43, 44).

TYPE LOCALITY: Shallow coastal waters of the NW Black Sea, Kazachya Bay, Crimean Peninsula (44.572967 N, 33.404199 E).

AUTHENTIC STRAIN: IBSS-Cr-7S4 (stable diplomorph) deposited at the Culture Collection of Marine Algae (CCMA) of IBSS and maintained on a regular basis at the Culture Collection of the Black Sea Cryptophytes (CCBSC) in the Department of Aquaculture and Marine Pharmacology of IBSS; *Storeatula* sp. 2 strain SZN-C14 (diplomorph) and *Rhodomonas* sp. 3, strain SZN-C42 (haplomorph), both isolated from the Gulf of Naples, Mediterranean Sea, Italy.

HABITAT: Marine coastal shallow waters.

ETYMOLOGY: The epithet refers to the fusiform cell shape characteristic of the species.

GENE SEQUENCE DATA: strain IBSS-Cr-7S4, nuclear 18S-ITS/5.8S-28S rRNA (PP578205), nucleomorph 18S rRNA (PV939381); *Rhodomonas* sp. 3 SZN-42, 18S rRNA (OQ878392); *Storeatula* sp. 2 T1 nuclear 18S rRNA (OQ878393).

MOLECULAR SIGNATURE: Autapomorphies in the nuclear 18S rDNA: 5′-TAGTGGCA **T**ATATCTTT<+420 bp upstream>-3′; 5′-ACCTTGG **T**ATTTAT<+84 bp upstream>-3′; 5′-TTATTT **A**CCTTGGTT<+73 bp upstream>-3′ (autapomorphic sites are bolded and underlined).

DIAGNOSTIC MOLECULAR CHARACTERS: ITS2′s helix I: [5′-UCACCUUAUCUCUGAUAAGCGUGG-3′] [((((((((((…)))))).))))].

ITS2′s helix II: [5′-GAGUAUCAUGCUUGCAAAAG CACGUUGCUC-3′] [((((… (((((….))))) …))))].

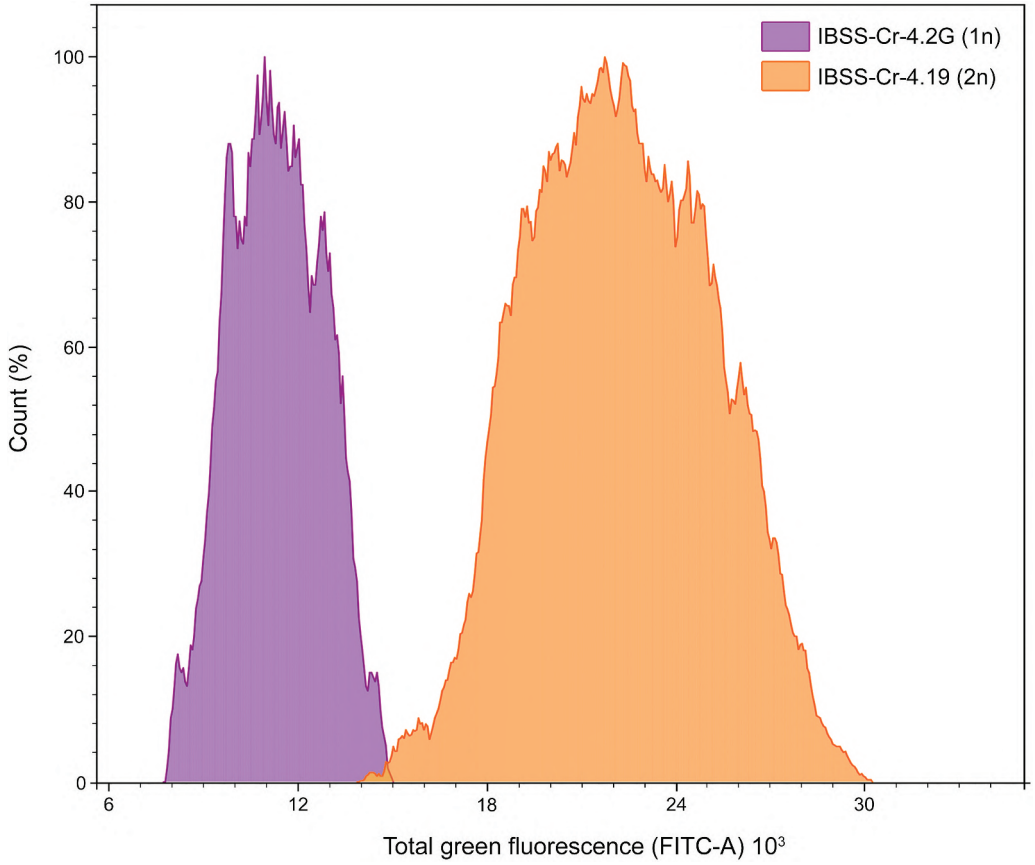


Fig. 48. Comparative flow cytometric analysis of cellular DNA content in *Eomonas vitalis* sp. nov. Histograms represent the distribution of cell counts relative to SYBR Green I fluorescence intensity (FITC-A channel). A twofold difference in fluorescence between the divergent morphotypes indicates different ploidy levels and confirms the dimorphic haploid-diploid life cycle of the species.

ITS2′s helix III: [5′-GUAGCGGACCAUGACUCA CGUAUCUGAGGUGCCCGUGAUGUAGCAGCC-UUUUUUAAAGGAGCAACAUCAUCGGCAACA-AAGCCUCAAGUACCACUAUUGAGACUCGGGU-AUCAGUACUCCUAC-3′]
[(((((.((((((.((((((((((.((((((((.((((((. . .)))))).)).)))))))).))) . . . . .)))))).)))))) . . . .)))).)))))) . . . . . .)).)))))].
ITS2′s helix IV: [5′-UUAAGUGUGUUUCACAC UUAG-3′] [((((((((((. . .))))))))))].

Eomonas marina (P.A.Dangeard) Saburova, Khanaychenko, Nikolaeva & Aleoshin comb. nov.

BASIONYM: *Cryptomonas marina* P.A.Dangeard 1892: Le Botaniste 3: 32, pl. II, fig. 20

SYNONYM: *Rhodomonas marina* (P.A.Dangeard) Lemmermann 1903 *emend.* Daugbjerg & Devantier 2024: 791, figs 5–9

DIAGNOSIS: Cells elliptical, with truncated anterior in lateral view and rounded to pointed posterior, 14–22 µm long and 6–12 µm wide. Two flagella unequal in length emanate from vestibulum. Gullet-furrow system lined with ejectosomes. Single deeply lobed chloroplast, yellow-brown in colour, contains Cr-PE 545. Central pyrenoid encircled by starch grains. Tubular nucleomorph penetrates pyrenoid matrix. Inner periplast composed of rectangular plates with rounded edges. Mid-ventral band present. Nucleus in posterior end and contractile vacuole in anterior end.

EPITYPE (designated by Daugbjerg & Devantier, 2024): A stub with material of strain S18 prepared for SEM, deposited at the Natural History Museum of Denmark, ref. number C-A-99713.

LECTOTYPE (designated by Daugbjerg & Devantier, 2024): Dangeard, 1892: pl. II, fig. 20.

TYPE LOCALITY: Luc-sur-Mer, Calvados, Normandy, France.

AUTHENTIC STRAIN: Strain S18 isolated from the Disko Bay, western Greenland.

GENE SEQUENCE DATA: Strain S18, 18S rRNA, ITS/5.8S rRNA, 28S rRNA (PP829267).

MOLECULAR SIGNATURE: Autapomorphies in the nuclear 18S rRNA V4: 5′-GTCGGGCTCGGGGAG**AT**TGTCGGCCTTTGGTC GGAT**A**G**TT**TCTCCGGGCCTTTCTGCCTGGG**A**A CCCTATTC<+141 bp upstream>-3′ (autapomorphic sites are bolded and underlined).

DIAGNOSTIC MOLECULAR CHARACTERS (according to Daugbjerg & Devantier, 2024):
ITS2′s helix I: [5′-CAUCACCUAAAACCUCGGU UUUGGCGUGGAG-3′]
[(.((((((((((….)))))))).)))).)].
ITS2′s helix II: 5′-UGAGCGUCAUGGCUG-CCUUUGUUGGUAGCCAC GUCGGUCG-3′]
[((((.((… (((((((.… …)))))))) …)).)))].
ITS2′s helix III: [5′-GGUGACGCCUCACGACCGAA AGGUAUGUGGUG UGCCGUGAUGUAGCAGCCU UCUCGUAAGGAGCAACAUCAUCGUACAUUA AGCCAUAUGCCAUCAAGUAGGCGCGUGGUUU GCACU-3′]
[(((((.(((.(.((.((…. ((((((((((((((.(((((((.((.((((….)))))).)).))))))).)))))) ….)))))))))). . . . . .)))).).)))).).)))))].
ITS2′s helix IV: [5′-UUUAGGAGUAUUUAUACUC UUAGG-3′]
[((((((((((….))))))))))].

***Eomonas vitalis* Saburova, Khanaychenko, Nikolaeva, Rylkova, Berdieva, Meger & Aleoshin sp. nov.** (Fig. 14–37)

DIAGNOSIS: Dimorphic with stable, dissimilar haploid and diploid morphs within strains. In both stages, cells oblong ellipsoid, with convex dorsal surface and mostly flat ventral margin, rounded apex and antapex in ventral and dorsal views, and rhinose apex in lateral view, and prominent dorso-ventral compression. Two unequal flagella emerge from subapical vestibulum. Chloroplast single, parietal, deeply bilobed, light-brown in colour, contains Cr-PE 545. Central pyrenoid round, located dorsally, encircled by starch grains. Nucleomorph embedded in a chloroplast-envelope invagination into the pyrenoid. Gullet lined with ejectosomes. Nucleus located posteriorly.

HAPLOMORPH cells 14.1–20.1 µm long, 7.1–12.8 µm wide. Gullet-furrow complex 1/3 of the cell length, furrow long. Inner periplast component with ordered system of discrete, anteriorly stepped plates exhibiting a superficial honeycomb-like pattern. Mid-ventral band present, extending 1/2 of the cell length.

DIPLOMORPH cells 15–22.5 µm long, 7.5–13.8 µm wide. Vestibulum V-shaped, subapical, with fold depressed on the left side, furrow absent. Inner periplast component continuous sheet-like, with numerous small underlying ejectosomes. Mid-ventral band absent.

HOLOTYPE: SEM stub with material of the strain IBSS-Cr-4.2G (stable haplomorph strain) (fixed and critical-point dried) deposited at the Algal Herbarium (LE) of the Komarov Botanical Institute, St. Petersburg, Russia (ref. number A0004145).

PARATYPE: SEM stub with material of the strain IBSS-Cr-4.19 (stable diplomorph strain) (fixed and critical-point dried) deposited at the Algal Herbarium (LE) of the Komarov Botanical Institute, St. Petersburg, Russia (ref. number A0004144). The glutaraldehyde and alcohol-fixed samples of the strains IBSS-Cr-4.2G and IBSS-Cr-4.19 are also kept in the Department of Aquaculture and Marine Pharmacology of IBSS under accession number A187-1-Cr-4.2G, A187-2-Cr-4.2G, A261-1-Cr-4.19 and A261-2-Cr-4.19, respectively.

TYPE LOCALITY: Shallow coastal waters of the NW Black Sea, Kazachya Bay, Crimean Peninsula (44.577384N, 33.407890E).

HABITAT: Marine coastal shallow waters.

AUTHENTIC STRAIN: Strains IBSS-Cr-4.2G (haplomorph) and IBSS-Cr-4.19 (diplomorph) are deposited at the Culture Collection of Marine Algae (CCMA) of IBSS and maintained on a regular basis at the Culture Collection of the Black Sea Cryptophytes (CCBSC) in the Department of Aquaculture and Marine Pharmacology of IBSS.

ETYMOLOGY: The epithet ‘*vitalis*’ (Latin for ‘pertaining to life’ or ‘vital’) is chosen both to honour the memory of our colleague and friend, Dr Vitaly Giragosov, who assisted in samples collection, and to reflect the remarkable vitality of this species’ cells under stressful conditions.

GENE SEQUENCE DATA: Strain IBSS-Cr-4.2G, nuclear 18S-ITS/5.8S-28S rRNA (PP578204) and nucleomorph 18S rRNA (PV939379); strain IBSS-Cr -4.19, nuclear 18S-ITS/5.8S-28S rRNA (PP578206) and nucleomorph 18S rRNA (PV939380).

MOLECULAR SIGNATURE: Autapomorphy in the nuclear 18S rRNA: 5′-TGCCCTTA**C**ATGTTCTG< +286 bp upstream>-3′ (autapomorphic site is bolded and underlined).

DIAGNOSTIC MOLECULAR CHARACTERS:
ITS2′s helix I: [5′-UCACUCCAAACUCUUGUG CUCUGCACGGGGGUUGAGACGUGA-3′][(((((((. ((((((((((…)))))))))))).)).)))))].
ITS2′s helix II: [5′-UGGGCAACAUGAGUUACUA UUCACGUUGC
CUG-3′] [(((((((((.(((((….)))))).)))))))))].
ITS2′s helix III: [5′-AAAAUGAAGGUCUACAG CUCACAUCAGCUAGUAUUGCGGUGUGCUGU-GAUGUAGCAGCCUUGUUUCAAGGACGGCCA-CAUCAUCGCACGAUUCAGCCGAAUGGCUCG-CCGGUGCGUGCAAUAAGUAGACCGACACUU-U-3′] [(((.((.(((((((.((… (((((.((.(((….((((((((.(((((((.((.(((((…)))))).)).)))))))).)))) … …)))) ….))).)).)))) …)) ….)))))))).)).)))].
ITS2′s helix IV: [5′-UUAAGGACUAGUU GAGGGUGGUUAUUGUUACUGCUCUCAAGCG-UCUUUAG-3′] [(((((((… (((((((((((… ….)))))))))))).)))))))].

Rhodomonas *complex*

Rhodomonas complex is herein treated as a monophyletic yet polymorphic assemblage corresponding to Clade B + C in the multi-locus molecular phylogeny (Fig. 42, Supplementary figs S2–S4). Of the four genera grouped within these clades, *Storeatula* is suppressed here as it represents the diplomorph stage of the life cycle (this study), while *Pyrenomonas* remains a long-standing heterotypic synonym of *Rhodomonas* (Hill & Wetherbee, 1989), and the morphological distinctions traditionally separating *Rhinomonas* from *Rhodomonas* are increasingly disputed due to their inconsistency across the group (Fig. 42) and susceptibility to preparation artefacts (Gantt, 1971; Santore, 1977; Kugrens & Lee, 1987; Novarino, 1991). Given the lack of discrete molecular boundaries and significant morphological overlap, *Rhinomonas* and *Rhodomonas* are considered herein to be treated as congeneric, a view supported by recent phylogenetic treatments (e.g. Majaneva *et al.*, 2014; Daugbjerg & Devantier, 2024). Under this unified framework, *Rhodomonas* Karsten 1898 remains the senior synonym with nomenclatural priority.

The *Rhodomonas* complex designated here contributes to the taxonomic stabilization of the family pending further formal revision. This status is maintained until the ongoing nomenclatural inconsistencies surrounding the generitype, *Rhodomonas baltica*, are fully resolved and the existing gap between morphological and molecular datasets is bridged. In the absence of stable morphological markers for this broad group, we provide the following molecular signatures to serve as a robust basis for delineating the lineage.

Molecular signatures

Hairpin 11 of the nuclear 18S rRNA exhibits one of five possible motifs: 5′-AACCACAGCC**C**TT**G**AGGT GGT-3′, 5′-AACCACAGCC**C**T**CGC**GGTGGT-3′, 5′-AACCACAGCC**C**TT**GC**GGTGGT-3′, 5′-AACCACA ACCTT**C**TGGTGGT-3′, or 5′-AACCACAACCTT **CGC**GGTGGT-3′ (apomorphic characters are bolded and underlined) (Fig. 44).

Symplesiomorphies in the nuclear 5.8S rRNA: 5′-ATG**T**TYY**TG**CATGAGCACGTCTGT**C**TGA<+53 bp upstream>-3′ (symplesiomorphic characters are bolded and underlined; only valid within the Pyrenomonadaceae) (Fig. 45).

Plesiomorphies in the nucleomorph 18S rRNA: 5′-GCTCGTAGTCGAAT-**T**-3′; 5′-**T**-TGGYGGCRGCG -3′; 5′-GCGTGAGTCAT-**T**-AACTCGCGC-3′ (plesiomorphic characters are bolded and underlined; only valid within the Pyrenomonadaceae).

DIFFERENTIAL DIAGNOSIS (only valid within the Pyrenomonadaceae): motif 5′-YGAC**T**YA**Y**GG-3′ in hairpin 10 of 18S rRNA (Fig. 43).

Nomenclatural stabilization: Taxa with ambiguous status

Based on our taxonomic reappraisal of the Pyrenomonadaceae (Supplementary table S1), we recommend the discontinuation of several historical *Rhodomonas*/*Rhinomonas* species names due to persistent taxonomic ambiguity and the absence of matching molecular data. These taxa lack designated types and possess original descriptions that are insufficient for modern identification, making the designation of epitypes or a definitive link to newly isolated strains challenging, if not impossible. To maintain nomenclatural stability, the following names are proposed to be treated as confused species and their use suspended pending definitive molecular confirmation from topotype material and the emendation of their morphological descriptions:
Rhodomonas gracilis J.Schiller 1926 nom. confus.;
Rhodomonas pelagica Lohmann 1908 *nom. confus.*;
Rhodomonas pusilla (H.Bachmann) Javornický 1967 nom. confus.;
Rhodomonas radix Javornický 2001 nom. confus.;
Rhodomonas rubra Geitler 1922 nom. confus.;
Rhodomonas ruttneri J.Schiller 1926 nom. confus.;
Rhodomonas tenuis Skuja 1948 nom. confus.;
Rhinomonas fragarioides (Butcher) D.R.A.Hill & R.Wetherbee 1988 nom. confus.;
Rhinomonas fulva (Butcher) D.R.A.Hill & R.Wetherbee 1988 nom. confus.;
Rhinomonas lateralis (Butcher) D.R.A.Hill & R.Wetherbee 1988 nom. confus.

Revision of the* Rhodomonas salina *complex

Molecular analysis revealed a highly supported subclade (0.99/100) within Clade C, comprising strains assigned to seven taxonomically accepted taxa: *Rhodomonas chrysoidea, R. salina, R. maculata, R. falcata, Rhinomonas reticulata, Rhin. reticulata* var. *atrorosea* and *Pyrenomonas helgolandii* (Fig. 42). The negligible genetic divergence in nuclear SSU and ITS rDNA sequences within this cluster indicates that these disparate morphotypes represent a single evolutionary lineage. Consequently, we propose the synonymization of these taxa, as their observed morphological diversity reflects high intraspecific variability and phenotypic plasticity rather than distinct taxonomic entities.

In accordance with the Principle of Priority (Article 11 of the ICN), *Rhodomonas salina* (Wisłouch) D.R.A.Hill & Wetherbee 1989 is

recognized as the correct name for this taxon, as its basionym (*Cryptomonas salina* Wisłouch 1924) represents the earliest validly published name within the group. This integration of molecular and phenotypic data resolves long-standing taxonomic inconsistencies (e.g. Santore 1986; Hill & Wetherbee, 1989; Novarino, 1991; Daugbjerg & Devantier, 2024) and clarifies the boundaries of this complex by treating the other names as heterotypic synonyms. This taxonomic adjustment results in the emendation of the diagnosis for *R. salina* to account for the broad morphological spectrum previously attributed to the synonymized taxa.

***Rhodomonas salina* (Wisłouch) D.R.A.Hill & R.Wetherbee 1989 emend.**

BASIONYM: *Cryptomonas salina* Wisłouch 1924: Acta Societatis Botanicorum Poloniae 2: 116, fig. 5.

EMENDED DIAGNOSIS: Cells are highly variable in shape and size, 8–19 µm in length and 4.5–11 µm in width. Cell shape varies from broadly ovoid or ellipsoidal to distinctly fusiform or asymmetric, often with a slightly pointed or rounded posterior and a truncate or rhinose anterior apex. Vestibulum narrow, funnel-like, opening at the centre of anterior; gullet-furrow complex 1/3 to 1/2 of the cell length lined with 2–4 rows of ejectosomes; furrow short, vertical. Chloroplast single, parietal, deeply bilobed, occupying about 3/4 of the cell periphery, with smooth to undulate margin, ranging in colour from olive-green to reddish-brown, containing Cr-PE 545. Pyrenoid single, central, ranging from conspicuous to faint or almost invisible, completely or partially encircled by starch grains. Nucleus in the posterior part of the cell. The inner periplast component consists of discrete rectangular plates with rounded corners, spirally arranged in transverse and longitudinal rows, appearing superficially as a honeycomb-like pattern with hexagonal arrangement of small trichocysts. The surface periplast component fibrillar. Mid-ventral band present. Nucleomorph is embedded into the pyrenoid.

Acknowledgements

We are grateful to our colleagues, IBSS researchers, N.A. Moiseeva and E.Y. Skorokhod, for giving us permission to present part of our joint spectrophotometry data on cryptophyte strains. We thank Dmitry V. Moiseenko for technical assistance in microalgae cultivation and Vyacheslav N. Lishaev (IBSS) for assistance with SEM. We would like to express our gratitude to the Editor and three anonymous reviewers for their meticulous review of our manuscript and their insightful comments and suggestions, which have significantly contributed to enhancing the overall quality of the manuscript.

Disclosure statement

No potential conflict of interest was reported by the author(s).

Funding

Research funding: This work was financially supported by the Research Program of the Russian Academy of Sciences grant agreement [# 124022400152-1, # 126021016953-0, and # 124030100106-2] at the IBSS RAS (AK, OR, YM, and TE) and the state assignment of Lomonosov Moscow State University (ON, VA).

Data availability statement

The DNA sequences reported in this study have been deposited in GenBank under accession numbers PP578204—PP578206 and PV939379—PV939381. All other relevant data supporting the findings of this study, including multiple sequence alignments used for phylogenetic reconstruction, high–resolution phylogenetic trees, detailed taxonomic summary table and distance matrix are available in the Supplementary Materials.

Supplementary material

The following supplementary material is accessible via the Supplementary Content tab on the article's online page at https://doi.org/10.1080/09670262.2026.2696474

Supplementary table S1. Taxonomic summary of the family Pyrenomonadaceae.
Supplementary table S2. Pairwise genetic p-distances among Pyrenomonadaceae lineages.
Supplementary fig. S1. Flask cultures of the new Black Sea cryptophyte strains at the end of exponential growth.
Supplementary fig. S2. Bayesian phylogenetic tree based on 18S rDNA gene sequences of the Pyrenomonadaceae members.
Supplementary fig. S3. Maximum likelihood (ML) tree based on ITS/5.8S rDNA gene sequences of the Pyrenomonadaceae.
Supplementary fig. S4. Bayesian phylogenetic tree based on nucleomorph 18S rRNA gene sequences of the Pyrenomonadaceae.
Supplementary file S1. Multiple sequence alignment of the nuclear-encoded rDNA operon (18S, ITS1, 5.8S, ITS2, and 28S rRNA).
Supplementary file S2. Multiple sequence alignment of the nucleomorph-encoded 18S rDNA.

Author contributions

M. Saburova: conceptualization, data curation; investigation; drafting and editing manuscript; A.N. Khanaychenko: original concept; formal analysis; funding acquisition; resources; methodology; investigation; culture maintenance; drafting and editing manuscript; O.V. Nikolaeva: data curation; formal analysis; methodology; molecular analysis; drafting and editing manuscript; O.A. Rylkova: methodology; electron microscopy; drafting and editing manuscript; T. Efimova: methodology; pigment analyses; editing manuscript; M. Berdieva: methodology; electron microscopy; editing manuscript; Y. Meger: methodology; flow cytometry; editing manuscript; V.V. Aleoshin: original concept; data curation; resources; analysis of molecular data; drafting and editing manuscript.

ORCID

Maria Saburova http://orcid.org/0000-0002-2204-2485
Antonina N. Khanaychenko http://orcid.org/0000-0002-4334-9996
Olga A. Rylkova http://orcid.org/0000-0002-2528-6223
Tatiana Efimova http://orcid.org/0000-0003-3908-4160
Mariia Berdieva http://orcid.org/0000-0002-5467-2713
Yakov Meger http://orcid.org/0000-0002-3413-8476
Vladimir V. Aleoshin http://orcid.org/0000-0002-3299-9950

References

Altenburger, A., Blossom, H.E., Garcia-Cuetos, L., Jakobsen, H.H., Carstensen, J., Lundholm, N., Hansen, P.J., Moestrup, Ø. & Haraguchi, L. (2020). Dimorphism in cryptophytes – the case of *Teleaulax amphioxeia/Plagioselmis prolonga* and its ecological implications. *Science Advances*, **6**(**eabb1611**): 1–9.

Andersen, R.A. (2005). *Algae Culturing Technique*. Elsevier Academic Press, New York.

Bistricki, T. & Munawar, M. (1978). A rapid preparation method for scanning electron microscopy of Lugol preserved algae. *Journal of Microscopy*, **114**: 215–218.

Bourrelly, P. (1970). *Les Algues d'Eau Douce. Tome III: Les Algues Bleues Et Rouges. Les Eugleniens, Peridiniens Et Cryptomonadines*. Editions N. Boubee & Cie, Paris.

Butcher, R.W. (1967). *An Introductory Account of the Smaller Algae of British Coastal Waters. IV. Cryptophyceae*. Fishery Investigations Series IV, Her Majesty's Stationery Office, London.

Caisová, L., Marin, B. & Melkonian, M. (2011). A close-up view on ITS2 evolution and speciation – a case study in the Ulvophyceae (Chlorophyta, Viridiplantae). *BMC Evolutionary Biology*, **11**: 62.

Caisová, L., Marin, B. & Melkonian, M. (2013). A consensus secondary structure of ITS2 in the Chlorophyta identified by phylogenetic reconstruction. *Protist*, **164**: 482–496.

Cavalier-Smith, T. (1993). Kingdom Protozoa and its 18 phyla. *Microbiological Review*, **57**(**4**): 953–994.

Cavalier-Smith, T., Couch, J.A., Thorsteinsen, K.E., Gilson, P., Deane, J.A., Hill, D.R.A. & McFadden, G.I. (1996). Cryptomonad nuclear and nucleomorph 18S rRNA phylogeny. *European Journal of Phycology*, **31**: 315–328.

Cerino, F. & Zingone, A. (2006). A survey of cryptomonad diversity and seasonality at a coastal Mediterranean site. *European Journal of Phycology*, **41**: 363–378.

Christensen, T. (1962). Alger. In *Botanik: bind II. systematisk botanik* (Bocher, T., Lange, M. & Sørensen, T., eds.), 1–178. nr. 2. I kommission hos Munksgaard, København.

Clay, B.L., Kugrens, P. & Lee, R.E. (1999). A revised classification of Cryptophyta. *Botanical Journal of the Linnean Society*, **131**: 131–151.

Coleman, A.W. (2000). The significance of a coincidence between evolutionary landmarks found in mating affinity and a DNA sequence. *Protist*, **151**: 1–9.

Coleman, A.W. (2007). Pan-eukaryote ITS2 homologies revealed by RNA secondary structure. *Nucleic Acids Research*, **35**: 3322–3329.

Cunningham, B.R., Greenwold, M.J., Lachenmyer, E.M., Heidenreich, K.M., Davis, A.C., Dudycha, J.L. & Richardson, T.L. (2019). Light capture and pigment diversity in marine and freshwater cryptophytes. *Journal of Phycology*, **55**: 552–564.

Dangeard, P.A. (1892). Sur un *Cryptomonas marina*. *Le Botaniste*, **3**: 32.

Daugbjerg, N. & Devantier, C.B. (2024). Emendation of *Rhodomonas marina* (Cryptophyceae): insights from morphology, molecular phylogeny and water-soluble pigment in an Arctic isolate. *Algae*, **39**(**2**): 75–96.

Deane, J.A., Strachan, I.M., Saunders, G.W., Hill, D.R. & McFadden, G.I. (2002). Cryptomonad evolution: nuclear 18S rDNA phylogeny versus cell morphology and pigmentation. *Journal of Phycology*, **38**: 1236–1244.

Dolgin, A. & Adolf, J. (2019). Scanning electron microscopy of phytoplankton: achieving high quality images through the use of safer alternative chemical fixatives. *Journal of Young Investigators*, **37**: 1–9.

Ehrenberg, C.G. (1832). Uber die Entwicklung und Lebensdauer der Infusionsthieve, nebst ferneren Beitragen zu einer Vergleichung ihrer organischen System. *Abhandlungen der Koniglichen Akademie der Wissenschaften in Berlin*, **1831**: 1–154.

Erata, M. & Chihara, M. (1989). Re-examination of *Pyrenomonas* and *Rhodomonas* (class Cryptophyceae) through ultrastructural survey of red pigmented cryptomonads. *Botanical Magazine [Shokubutsu-Gaku Zasshi] Tokyo*, **102**(**3**): 429–443.

Gantt, E. (1971). Micromorphology of the periplast of *Chroomonas* sp. (Cryptophyceae). *Journal of Phycology*, **7**: 177–184.

Gillott, M.A. & Gibbs, S.P. (1980). The cryptomonad nucleomorph: its ultrastructure and evolutionary significance. *Journal of Phycology*, **16**: 558–568.

Greenwold, M.J., Merritt, K., Richardson, T.L. & Dudycha, J.L. (2023). A three-genome ultraconserved element phylogeny of Cryptophytes. *Protist*, **174**(**6**): 125994.

Gusev, E., Martynenko, N., Kulizin, P. & Kulikovskiy, M. (2022). Molecular diversity of the genus *Cryptomonas* (Cryptophyceae) in Russia. *European Journal of Phycology*, **57**(**4**): 526–550.

Gusev, E., Podunay, Y., Martynenko, N., Shkurina, N. & Kulikovskiy, M. (2020). Taxonomic studies of *Cryptomonas lundii* clade (Cryptophyta: Cryptophyceae) with description of a new species from Vietnam. *Fottea Olomouc*, **20**(**2**): 137.

Hall, T.A. (1999). BioEdit: a user-friendly biological sequence alignment editor and analysis program for Windows 95/98/NT. *Nucleic Acids Symposium Series*, **41**: 95–98.

Hill, D.R.A. (1991). A revised circumscription of *Cryptomonas* (Cryptophyceae) based on examination of Australian strains. *Phycologia*, **30**: 170–188.

Hill, D.R.A. & Rowan, K.S. (1989). The biliproteins of the Cryptophyceae. *Phycologia*, **28**: 455–463.

Hill, D.R.A. & Wetherbee, R. (1986). *Proteomonas sulcata* gen. et sp. nov. (Cryptophyceae), a cryptomonad with two morphologically distinct and alternating forms. *Phycologia*, **25**(**4**): 521–543.

Hill, D.R. & Wetherbee, R. (1988). The structure and taxonomy of *Rhinomonas pauca* gen. et sp. nov. (Cryptophyceae). *Phycologia*, **27**(**3**): 355–365.

Hill, D.R. & Wetherbee, R. (1989). A reappraisal of the genus *Rhodomonas* (Cryptophyceae). *Phycologia*, **28**(**2**): 143–158.

Hoef-Emden, K. (2007). Revision of the genus *Cryptomonas* (Cryptophyceae) II: incongruences between the classical morphospecies concept and

molecular phylogeny in smaller pyrenoid-less cells. *Phycologia*, **46**(**4**): 402–428.
Hoef-Emden, K. (2012). Pitfalls of establishing DNA barcoding systems in protists: the Cryptophyceae as a test case. *PLOS ONE*, **7**(**8**): e43652.
Hoef-Emden, K. (2018). Revision of the genus *Chroomonas* Hansgirg: the benefits of DNA-containing specimens. *Protist*, **169**: 662–681.
Hoef-Emden, K. & Archibald, J.M. (2017). Cryptophyta (Cryptomonads). In *Handbook of the protists* (Archibald, J.M., Simpson, A.G.B. & Slamovits, C.H., eds.), 851–891. Springer International Publishing, Cham, Switzerland.
Hoef-Emden, K., Marin, B. & Melkonian, M. (2002). Nuclear and nucleomorph SSU rDNA phylogeny in the Cryptophyta and the evolution of cryptophyte diversity. *Journal of Molecular Evolution*, **55**: 161–179.
Hoef-Emden, K., Melkonian, K., Martel Quintana, A., Pérez Reyes, C., Rancel Rodríguez, N.M., Melkonian, B. & Melkonian, M. (2024). Diversity of cryptophyte cultures from the Canary Islands. *Phycologia*, **63**(**3**): 312–316.
Hoef-Emden, K. & Melkonian, M. (2003). Revision of the genus *Cryptomonas* (Cryptophyceae): a combination of molecular phylogeny and morphology provides insights into a long-hidden dimorphism. *Protist*, **154**: 371–409.
IOCCG Protocol Series. (2018). Inherent optical property measurements and protocols: absorption coefficient. In *Ocean optics and biogeochemistry protocols for satellite ocean colour sensor validation* (Neeley, A.R. & Mannino, A., eds.), 1–78. Vol. **1.0**. IOCCG, Dartmouth.
Karsten, G. (1898). *Rhodomonas baltica*, n.g. et sp. *Wissenschaftliche Meeresuntersuchungen, Abteilung Kiel, Neue Folge*, **3**: 15–16.
Katoh, K., Rozewicki, J. & Yamada, K.D. (2019). MAFFT online service: multiple sequence alignment, interactive sequence choice and visualization. *Briefings in Bioinformatics*, **20**: 1160–1166.
Khanaychenko, A.N., Nikolaeva, O.V., Rylkova, O.A., Saburova, M. & Aleoshin, V.V. (2024). Genus *Proteomonas* is not monotypic: *P. agilis* sp. nov. (Cryptophyceae, Geminigeraceae) from the Black Sea and hidden diversity of *Proteomonas* species. *Botanica Marina*, **67**(**6**): 621–636.
Khanaychenko, A.N., Rylkova, O.A., Aganesova, L.O., Popova, O.V., Aleoshin, V.V. & Saburova, M. (2022). *Rhodomonas storeatuloformis* sp. nov. (Cryptophyceae, Pyrenomonadaceae), a new cryptomonad from the Black Sea: morphology versus molecular phylogeny. *Fottea Olomouc*, **22**(**1**): 122–136.
Kjer, K.M., Blahnik, R.J. & Holzenthal, R.W. (2001). Phylogeny of Trichoptera (Caddisflies): characterization of signal and noise within multiple datasets. *Systematic Biology*, **50**(**6**): 781–816.
Klaveness, D. (1985). Classical and modern criteria for determining species of Cryptophyceae. *Bulletin of the Plankton Society of Japan*, **32**: 111–128.
Kugrens, P., Clay, B.L. & Lee, R.E. (1999). Ultrastructure and systematics of two new freshwater red cryptomonads, *Storeatula rhinosa*, sp. nov. and *Pyrenomonas ovalis*, sp. nov. *Journal of Phycology*, **35**(**5**): 1079–1089.
Kugrens, P. & Lee, R.E. (1987). An ultrastructural survey of cryptomonad periplasts using quick-freezing freeze-fracture techniques. *Journal of Phycology*, **23**: 365–376.
Lane, C.E. & Archibald, J.M. (2008). New marine members of the genus *Hemiselmis* (Cryptomonadales, Cryptophyceae). *Journal of Phycology*, **44**: 439–450.
Lane, C.E., Khan, H., MacKinnon, M., Fong, A., Theophilou, S. & Archibald, J.M. (2005). Insight into the diversity and evolution of the cryptomonad nucleomorph genome. *Molecular Biology and Evolution*, **23**(**5**): 856–865.
Lazăr, L., Boicenco, L., Marin, O., Culcea, O., Pantea, E., Bişinicu, E., Timofte, F. & Mihailov, M.-E. (2018). Black Sea eutrophication dynamics from causes to effects. *Cercetări Marine-Recherches Marines*, **48**(**1**): 100–117.
Magalhães, K.F.L. (2018). Taxonomy and molecular phylogeny of Cryptophyceae (Cryptophyta) from cultures. PhD Thesis, Universidade de São Paulo, São Paulo.
Majaneva, M., Remonen, I., Rintala, J.M., Belevich, I., Kremp, A., Setälä, O., Jokitalo, E. & Blomster, J. (2014). *Rhinomonas nottbecki* n. sp. (Cryptomonadales) and molecular phylogeny of the family Pyrenomonadaceae. *Journal of Eukaryotic Microbiology*, **61**(**5**): 480–492.
Marin, B., Klingberg, M. & Melkonian, M. (1998). Phylogenetic relationships among the Cryptophyta: analyses of nuclear-encoded SSU rRNA sequences support the monophyly of extant plastid-containing lineages. *Protist*, **149**(**3**): 265–276.
Martynenko, N.A., Gusev, E.S., Sterlyagova, I.N. & Kulikovskiy, M.S. (2022). Revealing hidden diversity in the *Cryptomonas erosa* clade (Cryptophyceae), with the description of two new species from acidic habitats. *Phycologia*, **61**(**2**): 184–194.
Medina, M., Collins, A.G., Silberman, J.D. & Sogin, M.L. (2001). Evaluating hypotheses of basal animal phylogeny using complete sequences of large and small subunit rRNA. *Proceedings of the National Academy of Sciences of the United States of America*, **98**(**17**): 9707–9712.
Medlin, L., Elwood, H.J., Stickel, S. & Sogin, M.L. (1988). The characterization of enzymatically amplified eukaryotic 16S-like rRNA-coding regions. *Gene*, **71**(**2**): 491–499.
Mikaelyan, A.S., Pautova, L.A. & Fedorov, A.V. (2021). Seasonal evolution of deep phytoplankton assemblages in the Black Sea. *Journal of Sea Research*, **178**: 102125.
Moncheva, S., Gotsis-Skretas, O., Pagou, K. & Krastev, A. (2001). Phytoplankton blooms in Black Sea and Mediterranean coastal ecosystems subjected to anthropogenic eutrophication: similarities and differences. *Estuarine Coastal and Shelf Science*, **53**(**3**): 281–295.
Nguyen, L.T., Schmidt, H.A., Von Haeseler, A. & Minh, B. Q. (2015). IQ-TREE: a fast and effective stochastic algorithm for estimating maximum-likelihood phylogenies. *Molecular Biology and Evolution*, **32**: 268–274.
Novarino, G. (1991). Observations on *Rhinomonas reticulata* comb. nov. and *Rhinomonas reticulata* var. *eleniana* var. nov. (Cryptophyceae), with comments on the genera *Pyrenomonas* and *Rhodomonas*. *Nordic Journal of Botany*, **11**: 243–252.
Novarino, G. (2005). Nanoplankton protists from the western Mediterranean Sea. II. Cryptomonads (Cryptophyceae = Cryptomonadea). *Scientia Marina*, **69**(**1**): 47–74.
Novarino, G. & Lucas, I.A.N. (1993). A comparison of some morphological characters in *Chroomonas ligulata* sp. nov. and *C. placoidea* sp. nov. (Cryptophyceae). *Nordic Journal of Botany*, **13**: 583–591.
Novarino, G. (2012). Cryptomonad taxonomy in the 21st century: the First 200 Years. In *Phycological Reports: Current Advances in Algal Taxonomy and Its Applications: Phylogenetic, Ecological and Applied Perspective* (Wolowski, K., Kaczmarska, I., Ehrman, J.E. & Wojtal, A.Z., eds.), 19–52. Institute of Botany, Polish Academy of Sciences, Krakow.

Pascher, A. (1914). Über Flagellaten und Algen. *Berichte Der Deutschen Botanischen Gesellschaft*, **32**: 136–160.

PerkinElmer, Inc. (2000). Lambda 25, 35, 45 User's Guide. Doc. No. 09934586. PerkinElmer, Inc. Waltham.

Pringsheim, E.G. (1944). Some aspects of taxonomy in the Cryptophyceae. *New Phytologist*, **43**: 143–150.

Ronquist, F., Teslenko, M., van der Mark, P., Ayres, D.L., Darling, A., Höhna, S., Larget, B., Liu, L., Suchard, M.A. & Huelsenbeck, J.P. (2012). MrBayes 3.2: efficient Bayesian phylogenetic inference and model choice across a large model space. *Systematic Biology*, **61**: 539–542.

Rouchijajnen, M.I. (1967). Species nova generis *Cryptomonas* (Pyrrophyta) e mari Nigro (Ponto Euxino). *Novitates Systematicae Plantarum Non Vascularium/Novosti Sistematiki Nizshikh Rastenii*, **4**: 71–73. (in Russian, with Latin diagnosis).

Rouchijajnen, M.I. (1970). Species novae generum *Cryptomonas* (Pyrrophyta) et *Platymonas* (Chlorophyta, Chlamydomonadales) e mari Nigro. *Novitates Systematicae Plantarum Non Vascularium/Novosti Sistematiki Nizshikh Rasteniii*, **7**: 20–23. (in Russian, with Latin diagnosis).

Santore, U.J. (1977). Scanning electron microscopy and comparative micromorphology of the periplast of *Hemiselmis rufescens, Chroomonas* sp., *Chroomonas salina* and members of the genus *Cryptomonas* (Cryptophyceae). *British Phycological Journal*, **12**(**3**): 255–270.

Santore, U.J. (1984). Some aspects of taxonomy in the Cryptophyceae. *New Phytologist*, **98**: 627–646.

Santore, U.J. (1986). The ultrastructure of *Pyrenomonas heteromorpha* comb. nov. (Cryptophyceae). *Botanica Marina*, **29**: 75–82.

Shalchian-Tabrizi, K., Bråte, J., Logares, R., Klaveness, D., Berney, C. & Jakobsen, K.S. (2008). Diversification of unicellular eukaryotes: cryptomonad colonizations of marine and fresh waters inferred from revised 18S rRNA phylogeny. *Environmental Microbiology*, **10**: 2635–2644.

Simdyanov, T.G., Diakin, A.Y. & Aleoshin, V.V. (2015). Ultrastructure and 28S rDNA phylogeny of two gregarines: *Cephaloidophora* cf. *communis* and *Heliospora* cf. *longissima* with remarks on gregarine morphology and phylogenetic analysis. *Acta Protozoologica*, **54**(**3**): 241–262.

Simdyanov, T.G., Guillou, L., Diakin, A.Y., Mikhailov, K. V., Schrével, J. & Aleoshin, V.V. (2017). A new view on the morphology and phylogeny of eugregarines suggested by the evidence from the gregarine *Ancora sagittata* (Leuckart, 1860) Labbé, 1899 (Apicomplexa: Eugregarinida). *PeerJ*, **5**: e3354.

Solarska, M., Adamski, M. & Piątek, J. (2023). Complicated family relationships, or about taxonomic problems in the family Pyrenomonadaceae (Cryptophyceae). *Oceanological and Hydrobiological Studies*, **52**: 299–306.

Tamura, K., Stecher, G., Peterson, D., Filipski, A. & Kumar, S. (2013). MEGA6: molecular evolutionary genetics analysis version 6.0. *Molecular Biology and Evolution*, **30**: 2725–2729.

Temraleeva, A.D. & Bukin, Y.S. (2022). Morphology, molecular phylogeny, and species delimitation within microalgal genera *Eubrownia, Spongiococcum*, and *Chlorococcum* (Chlorophyceae, Chlorophyta). *South African Journal of Botany*, **151**: 396–409.

van den Hoff, J., Bell, E. & Whittock, L. (2020). Dimorphism in the Antarctic cryptophyte *Geminigera cryophila* (Cryptophyceae). *Journal of Phycology*, **56**(**4**): 1028–1038.

Van der Auwera, G., Chapelle, S. & De Wachter, R. (1994). Structure of the large ribosomal subunit RNA of *Phytophtora megasperma*, and phylogeny of the oomycetes. *FEBS Letters*, **338**: 133–136.

Wetherbee, R., Hill, D.R.A. & Brett, S.J. (1987). The structure of the periplast components and their association with the plasma membrane in a cryptomonad flagellate. *Canadian Journal of Botany*, **65**: 1019–1026.

Wisłouch, S. (1924). Przyczynek do biologji solnisk i genezy szlamow leczniczych na Krymie. *Acta Societatis Botanicorum Poloniae*, **2**(**2**): 99–129.

Wuyts, J., De Rijk, P., Van de Peer, Y. & Pison, G. (2000). Comparative analysis of more than 3000 sequences reveals the existence of two pseudoknots in area V4 of eukaryotic small subunit ribosomal RNA. *Nucleic Acids Research*, **28**(**23**): 4698–4708.

Zuker, M. (2003). Mfold web server for nucleic acid folding and hybridization prediction. *Nucleic Acids Research*, **31**: 3406–3415.